In: New Developments in the Standard Model
Editor: Ryan J. Larsen
ISBN: 978-1-61209-989-7

Chapter 1

TOWARDS ISO STANDARD EARTH IONOSPHERE AND PLASMASPHERE MODEL

Tamara Gulyaeva[1,*] and Dieter Bilitza[2]
[1]IZMIRAN, RAS, Troitsk, Moscow Region, Russia
[2]George Mason University, Fairfax, VA, US and
Goddard Space Flight Center,
Heliospheric Physics Laboratory,
Greenbelt, MD, US

Abstract

Space exploration has been identified by several governments as a priority for their space agencies and commercial industry. A good knowledge and specification of the ionosphere and plasmasphere are the key elements necessary to achieve this goal in the design and operation of space vehicles, remote sensing, reliable communication and navigation. The International Standardization Organization, ISO, recommends the International Reference Ionosphere (IRI) for the specification of ionosphere plasma densities and temperatures and lists several plasmasphere models for extending IRI to plasmaspheric altitudes, as described in the ISO Technical Specification, ISO/TS16457:2009. IRI is an international project sponsored jointly by the Committee on Space Research (COSPAR) and the International Union of Radio Science (URSI). The buildup of IRI electron density profile in the bottomside and topside ionosphere and its extension to the plasmasphere are discussed in the paper. The paper is also an important step towards the promotion of this model to full ISO standard. It includes a section on theoretical models used in data assimilation scenarios. The paper will introduce recent progress in IRI system developments, comparison of results provided by its different options and prospects of future improvements. Specification of the ionospheric weather index ranging from quiet conditions to severe storm in the ionosphere and plasmasphere is provided. Development of the ISO international standard would harmonize national approaches in this subject area that may serve as barriers to international trade. The ISO information will provide an open source model system to those organizations that are concerned with space vehicle design and operations, plasma environment specification, and communication / navigation services for the common specification of the Earth ionosphere and plasmasphere.

* E-mail address: gulyaeva@izmiran.ru

Keywords: International Reference Ionosphere, Plasmasphere, Standard Model, Electron Density, Total Electron Content

1. Introduction

The ionosphere and plasmasphere are conductive, ionized regions of the Earth's atmosphere consisting of free electrons and ions. The ionosphere and plasmasphere are embedded within the Earth's magnetic field and thus are constrained by interactions of the ionized particles with the magnetic field. The ionization levels in this near-Earth space plasma are controlled by solar extreme ultraviolet (EUV) radiation and particle precipitation. The dynamics of the neutral atmosphere plays a significant role in causing movement of the ionized particles by collisions with neutral atoms and molecules from the surrounding thermosphere. The ionosphere extends in altitude from about 65 km to 2000 km and exhibits significant variations with local time, altitude, latitude, longitude, solar cycle, season, and geomagnetic activity. At middle and low latitudes the ionosphere is contained within a region of closed field lines, whereas at high latitudes the geomagnetic field can reconnect with the interplanetary magnetic field and thus open the ionosphere to the driving force of the solar wind.

Plasma flowing upwards from the oxygen-dominated topside ionosphere remains at the lines of force co-rotating with the Earth and comprises the hydrogen-dominated plasmasphere extended up to a few Earth's radii (Carpenter and Park, 1973; Kotova, 2007). These two regions of upper atmosphere are strongly coupled through diffusion and resonant charge exchange reactions between O^+ and H^+. At quiet conditions, H^+ in the plasmasphere typically diffuses down to the topside ionosphere at night and undergoes resonant charge exchange reactions with atomic oxygen to produce O^+ (downward flux). The O^+ produced in this way can make a significant contribution to the maintenance of the nighttime ionosphere, and works in combination with the meridional component of the neutral wind. The depleted nighttime plasmasphere can be refilled during the day through the reverse process; that is, the O^+ ions flow up from the ionosphere, exchange charges with the neutral hydrogen atoms to produce protons, and the protons are then stored in the plasmasphere (upward flux). During geomagnetically disturbed conditions, the flux situation can be changed. Under these conditions, the plasmaspheric plasma can be eroded by the enhanced magnetospheric electric fields, and consequently, the flux becomes upward both during the day and night, due to the reduced plasmaspheric pressure, to refill the empty plasmaspheric flux tubes. While the low-latitude flux tubes refill relatively quickly due to their small volumes, most of the mid-latitude flux tubes are always in a partially depleted state, since the average time between consecutive geomagnetic storms is not long enough for the upflowing ionospheric flux to completely refill the flux tubes.

Terrestrial HF communications rely entirely on reflections from the ionized layers in the upper atmosphere, but the ionosphere also distorts Earth-space and spacecraft-to-spacecraft links. Although empirical models of the ionosphere are now accessible via electronic networking, most of them are far from reliable in predicting the average ionospheric conditions, not to mention their limitations in forecasting the ionospheric "space weather". In particular, a reliable and standard ionosphere-plasmasphere model is required for calibration of trans-ionospheric signals of the high altitude Global Positioning System (GPS) and Global

Navigation Satellite System (GLONASS) satellites at 20,200 km above the Earth which could in turn supply total electron content per m^2, TEC, in the column from the bottom of the ionosphere to the plasmapause.

For many years real-time updates of median ionospheric climatological models for various military and civilian users have been limited by the availability of globally distributed real-time ionospheric measurements. This situation has now improved greatly because of the increasing needs of civilian users for governing the operation of thousands of world-wide receivers of signals from GPS and other satellites navigational systems. Satellite navigation satellites such as GPS, Glonass, Galileo, can detect the delay due to the integrated total electron content (TEC) a radio signal is experiencing during its transit from spacecraft to receiver through the ionosphere. The ionospheric range error correction is required by the geodetic community which in turn is providing continuing flow of total electron content (TEC) data by simple Internet transfer to users anywhere in the world. There are still some limitations in coverage over the oceans. Uncertainties also remain in regards to accurately accounting for the plasmaspheric content and related to the techniques used to convert the slant path measurements into vertical TEC. A small uncertainty also remains due to difficulties to fully account for and determine the instrument bias factors for the ground receiver and satellite transmitter.

Ionospheric modeling using TECgps data has been the focus of numerous studies during the past decade. The range error caused by ionospheric delay in GPS signals is currently the largest component that affects the accuracy of positioning and navigation determination using single frequency GPS measurements. Ionospheric modeling is an effective approach for correcting the ionospheric range error and improving the GPS positioning accuracy. The abundance of GPS measurements from worldwide-distributed GPS reference networks, which provide 24-h uninterrupted operational services to record dual-frequency GPS measurements, provides an ideal data source for ionospheric modeling research.

Ionospheric remote sensing is in a rapid growth phase, driven by an abundance of ground and space-based GPS receivers and the advent of data assimilation techniques for space weather (Bust et al., 2004; Jorgensen et al., 2010). The horizontal resolution can be achieved by a local dense array of ground instruments such as GPS receivers. Vertical resolution can be achieved by GPS occultations for a constellation of satellites such as the current constellation observing system for meteorology ionosphere and climate (COSMIC) array (http://www.cosmic.ucar.edu). COSMIC system, a constellation of six satellites, nominally provides up to 3000 ionospheric occultations per day with an unprecedented global coverage of GPS occultation measurements (between 1400 and 2400 good soundings per day as of January 2010). Calibrated measurements of ionospheric delay, the total electron content or COSMIC-TEC measured from the satellite altitude to GPS orbit, suitable for input into assimilation models (Angling et al., 2004) are currently made available in near real-time from the COSMIC with a latency of 30 to 120 minutes. Similarly, TECgps data are available from worldwide networks of ground GPS receivers. The combined ground and space-based GPS datasets provide a new opportunity to more accurately specify the 3-dimensional ionospheric density with a time lag of only 15 to 120 minutes. It is, however, important to use these data cautiously and with awareness for limitations and uncertainties (Hysell, 2007; Kelley et al., 2009; Vergados and Pagiatakis, 2010; Liu et al, 2010).

TECgps data together with near real-time supply of the ionosonde data provide an outstanding capability for near world-wide monitoring and imaging of the ionosphere and

plasmasphere using the relevant model operating in assimilative regime (Bust and Mitchel, 2008; Scherliess et al., 2004). The TEC measurements can be used directly or organized into two-dimensional TEC maps to infer information on the horizontal structuring of the electron density. However, information on how plasma can be lifted to high altitudes and transported to other regions, polar outflow, and other vertical dynamical changes is lost with such simple mapping algorithms. In order to obtain information on the vertical structure of the electron density, its temporal variation, and transport, the three-dimensional time-evolving (hence four-dimensional) spatial field of electron density tomographic reconstruction is necessary. The International Reference Ionosphere extended to the plasmasphere is capable to serve as the initial condition (background ionosphere) in process of 3D tomographic imaging of electron density (Bust et al., 2001; Arikan et al., 2007).

A technique for IRI-2000 implementation for the near real-time US-TEC reconstruction of the three-dimensional distribution of electron density is developed with Gauss-Markov Kalman filtering of ground-based GPS observations (Fuller-Rowell et al., 2006). NOAA's TEC specification methodology (Gauss-Markov Kalman filter) over the continental United States has been expanded to the multi-regional domains and to the entire globe. The ensemble Kalman Filter (EnKF) is a Monte-Carlo approximation of a sequential Bayesian filtering process. Ensemble (Monte-Carlo) samples are used to estimate the covariance of the prior distribution of the model state and of observations. The algorithm consists of recursive application of an analysis (update) step in which the prior ensemble estimate of the state is updated by observations to produce a posterior (analysis), and a forecast step in which the posterior sample is propagated forward in time with a dynamical model to the next observation time. There is no need to compute explicitly the enormous prior covariance matrices that are associated with large dynamical models. The EnKF has been shown to work well with both nonlinear model dynamics and nonlinear relationships between observations and model state variables, and there is no need to linearize a forecast model or a forward (observation) operator. The resulting ease of implementation has led to a number of atmospheric assimilation applications by groups that may not have the resources to develop variational systems like those used for operational numerical weather prediction. To avoid filter divergence (in which ensemble samples diverge gradually from the truth or the observation) due to insufficient variance in the sample posterior/forecast covariance the sample forecast covariance is artificially inflated.

Due to highly temporal and spatial variability of space plasma surrounding the Earth and the requirements of its representation in the design and operation of space vehicles, remote sensing, reliable communication and navigation, modeling of the ionosphere and plasmasphere has been and still is a research focus within the worldwide space science communities. Among these efforts an outstanding part plays the International Reference Ionosphere (IRI) extended to the plasmasphere recognized as a candidate model for an international standard of the specification of ionosphere and plasmasphere plasma densities and temperatures by the International Standardization Organization, ISO (ISO/TS16457:2009).

The International Reference Ionosphere Project was established in 1968 jointly by the Committee on Space Research (COSPAR) and the International Union of Radio Science (URSI). The IRI is an observation-based climatological standard model of the ionosphere that is widely used to predict and mitigate the significant effects the ionosphere has on the performance of communication and global positioning systems. The model is designed to

provide vertical profiles of the main ionospheric parameters for suitably chosen locations over the globe, hours, seasons, and levels of solar activity, representing monthly mean conditions based on experimental evidence. The IRI Task Group brought together a distinguished team of experts representing the different ground and space measurement techniques and the different countries interested in ionospheric research. The truly international spirit of the IRI project is demonstrated by the typically more than 20 countries represented at the annual workshops jointly sponsored by COSPAR, URSI and IAGA (International Association on Geomagnetism and Aeronomy). A well balanced team both in terms of regional interest and in terms of science expertise is one of the secrets behind the success of the IRI mission.

One of the most challenging tasks in developing an empirical model is solving the right data question for regions and/or time periods where conflicting results exist for a certain parameter. Early measurements of plasma temperatures, for example, were difficult to interpret since the results of in-situ probes were up to a factor of two higher than observations by incoherent scatter radars. Improvements in probe design and in radar data reduction led to good agreement in the early seventies. In such cases much sensitivity and insight is required to get the experimenters to compare their results and to discuss possible error sources. The main sources of information on which the IRI system was built are the ground based and topside sounding ionosondes, incoherent scatter radars, in-situ rocket and satellite measurements (Bilitza et al., 1993a,b). Plasmaspheric electron densities have been obtained indirectly from trans-plasmaspheric VLF measurements (whistler) and from highly sensitive in-situ instruments. The improvement of the IRI representation of ionospheric parameters, such as electron density, electron temperature, ion composition and ion temperatures, and total electron content (TEC) through the ionosphere and plasmasphere still remains a challenge for the IRI Project.

In the next section we will briefly outline physical models which are important as tools to explore and understand the physical processes that shape the ionospheric environment.

2. Physical Models

Physical models typically use a numerical iterative scheme to solve the Boltzmann equations for the ionospheric gas including the continuity, energy, and momentum equations. They are solved along field-lines of the Earth magnetic field where the field is represented either by a simple tilted dipole or a multiplex model like the International Geomagnetic Reference Field (IGRF). Solving the equations along a full flux tube would take account of the plasmaspheric flux in a self-consistent way for a given geophysical condition, however, to keep control over the flux as a free parameter, the plasmaspheric flux is provided as a top boundary condition. The effects of the geomagnetic field on the transport of the ionospheric plasma are introduced by the magnetic dip (I) and declination (D) angles from the International Geomagnetic Reference Field (IGRF).

The ionosphere is strongly coupled with the neutral atmosphere, chemically as well as dynamically. In addition to the effects of the neutral wind, the neutral atmosphere significantly affects the ionospheric plasma density distribution through neutral composition and temperature. The neutral composition is a crucial factor not only for the production and loss of the plasma, but also for the diffusion of the ionospheric plasma through the neutral atmosphere. The neutral temperature effect on the ionosphere usually comes from the changes

of the neutral densities caused by the neutral temperature change. Below the F-region peak, chemical equilibrium prevails and the plasma density profile is largely controlled by the neutral composition through the production and loss. As altitude increases, plasma diffusion becomes important and well above the F-region peak, the plasma density profile is primarily determined by diffusion. However, the diffusion of the plasma through the neutral atmosphere strongly depends on the neutral densities, mainly the O density in the topside ionosphere, via collisions between the plasma and the neutrals.

A physical model requires several input parameters, including the neutral densities and temperature, neutral wind, and plasma temperatures. For these inputs, empirical models are adopted. In assimilative mode of operation, up to six free model parameters should be adjusted to measurements within physically reasonable ranges, and this cannot be reached straightforward under certain conditions.

For the last several years, Utah State University has been developing the Global Assimilative Ionospheric Model, GAIM (Scherliess et al., 2004; Wang et al., 2004a). GAIM uses a physics-based ionosphere-plasmasphere-polar wind model and a Kalman filter as a basis for assimilating a diverse set of real-time (or near real-time) measurements (Schunk and Nagy, 2000). GAIM is a data assimilation model that specifies and forecasts the state of the ionosphere. There are several versions of GAIM under development at USU. One version, a Gauss-Markov Kalman filter uses the Ionosphere Forecast Model as the background model specification. A second version of GAIM being developed by USU is a physics-based, reduced-state Kalman filter assimilation algorithm (Scherliess et al., 2004). This reduced-state approach was tested under simulation, though for the simulation only predictions of electron density obtained from the first principle model (with driver adjustment) were used. The full analyzed electron density and error covariance was not used in the simulation.

The University of Southern California and the Jet Propulsion Laboratory (USC/JPL) physics model (Pi et al., 2003; Hajj et al., 2004; Wang et al., 2004a) is derived from the Sheffield University Plasmasphere Ionosphere Model, SUPIM (Bailey et al., 1997). In physical models, such as SUPIM, the time-dependent equations of continuity, momentum (ignoring the time variation and inertial terms in the momentum equation), and energy balance are solved along eccentric-dipole magnetic field lines for the densities, field-aligned fluxes and temperatures of the ions and the electrons. Its application relies on accurate estimate of the solar EUV, ExB drift, neutral wind, and neutral densities. The ion momentum equation is further broken into a field-parallel and field perpendicular component. The velocity component perpendicular to the magnetic field is considered to be due entirely to ExB and is an input driver. The parallel component of velocity also has input drivers due to neutral winds and electron and ion temperatures. Thus in the USC/JPL system the only state variable solved for is the O^+ density; the rest are input drivers to the system.

The Coupled Thermosphere Ionosphere Model (CTIM) of Fuller-Rowell et al. (1996) was developed from the ionospheric part of the Sheffield model. As with many of the theoretical model, the global atmosphere is divided into a series of elements in geographic latitude, longitude, and pressure (or altitude). Each grid point rotates with Earth to define a non-inertial frame of reference in an Earth-centered coordinate system. The magnetoispheric input is provided with statistical models of auroral precipitation (Fuller-Rowell and Evans, 1987) and electric fields (Foster et al., 1986). Both inputs are keyed to a hemispheric power index (PI), based on the TIROS/NOAA auroral particle measurements. A recent upgrade of this model, including self-consistent plasmasphere and low latitude ionosphere models is in

the Coupled Thermosphere-Ionosphere-Plasmasphere model (CTIP; Millward et al. 1996). The effects of E×□B drift at lower latitudes are incorporated by the inclusion of an empirical low-latitude electric field model. The new ionosphere-plasmasphere component of CTIP solves the coupled equations of continuity, momentum and energy to calculate the densities, field-aligned velocities and temperatures of the ions O^+ and H^+ and the electrons, along a total of 800 independent flux-tubes arranged in magnetic longitude and L value (20 longitudes and 40 L values).

The Field Line Interhemispheric Plasma (FLIP) model (Richards, 1996) is a first-principles, one-dimensional, time-dependent, chemical, and physical model of the ionosphere and plasmasphere. It couples the local ionosphere to the overlying plasmasphere and conjugate ionosphere by solving the ion continuity and momentum, ion and electron energy, and photoelectron equations along entire magnetic flux tubes. The interhemispheric solutions yield densities and fluxes of H^+, O^+, He^+, and N^+ as well as the electron and ion temperatures.The neutral densities, temperature, and wind are supplied by the empirical MSIS (Hedin, 1991) and HWM (Hedin et al., 1996) models. During quiet times the error in the inputs for the solar EUV flux, MSIS neutral parameters, reaction rates, and cross sections are typically about 20%. During magnetic storms uncertainties may be much larger. The set of nonlinear, second-order, partial differential equations for continuity, momentum, and energy is transformed into finite difference equations and solved by a Newton-Raphson iterative scheme. The current FLIP model is basically a midlatitude model because it neglects convection electric fields, which are important at equatorial and auroral latitudes.

As described in the previous paragraphs driver inputs must be obtained from empirical models including the following: thermospheric densities from the Mass Spectrometer Incoherent Scatter model (Hedin, 1991), neutral winds from the horizontal wind model (Hedin et al., 1996), solar EUV as described by Tobiska (1991), electric fields (e.g., Fejer, 1991; Heppner and Maynard, 1987; Scherliess and Fejer, 1999), and electron energy precipitation flux (Fuller-Rowell and Evans, 1987). The interested reader can refer to Pi et al. (2003) and references therein. In the 2003 model validation experiment, only vertical drift at the geomagnetic equator was simulated and estimated, while all the other inputs were held at their empirical values. The vertical drift was parameterized by nine coefficients at different local times.

The Open Geospace General Circulation Model (OpenGGCM) is a global model of the magnetosphere-ionosphere system. It solves the magneto-hydrodynamic (MHD) equations in the outer magnetosphere and couples via field aligned current (FAC), electric potential, and electron precipitation to an ionosphere potential solver and the Coupled Thermosphere Ionosphere Model (CTIM) (Raeder et al., 2008). This code coupling enables studies of the global energy budget of the magnetosphere-ionosphere-thermosphere system. The CTIP model (Coupled Thermosphere Ionosphere – Plasmasphere) is a self-consistent first-principles model of the inner magnetosphere and thermosphere-ionosphere-plasmasphere system. It solves the continuity equations and the steady-state momentum equations for densities and velocities of O^+ and H^+ ions along the geomagnetic flux tubes using the finite difference schemes (Wang et al., 2004b).

The NCAR thermospheric general circulation model (TGCM) is extended to include a self-consistent aeronomic scheme of the thermosphere and ionosphere (Roble et al., 1988). The model now calculates total temperature, instead of perturbation temperature about some specified global mean, global distributions of N(2D), N(S) and NO, and a global ionosphere

with distributions of O^+, NO^+, $O2^+$, N•', N^+, electron density, and ion temperature as well as the usual fields of winds, temperature and major composition. Mutual couplings between the thermospheric neutral gas and ionospheric plasma occur at each model time step and at each point of the geographic grid. Steady state results for this first Eulerian model of the ionosphere are presented for solar minimum equinox conditions. The calculated thermosphere and ionosphere global structure agrees reasonably well with the structure of these regions obtained from empirical models. This suggests that the major physical and chemical processes that describe the large-scale structure of the thermosphere and ionosphere have been identified and a self-consistent aeronomic scheme, based on first principles, can be used to calculate thermospheric and ionospheric structure considering only external sources. Global empirical atmospheric models, such as the mass spectrometer/ incoherent scatter models (e.g., Hedin, 1991), were used to specify atmospheric properties for ionospheric model. Equations describing the ionosphere and thermosphere are both solved on the TGCM geographic grid. Ion drift for the ionospheric calculation is obtained from the empirical model of Richmond et al. (1980) for low- and mid-latitudes and the empirical model of Heelis et al. (1982) for high latitudes. Consideration of displaced geomagnetic and geographic poles is included. Results for solar minimum equinox conditions are presented that show good agreement with MSIS-86 (Hedin, 1991). The self-consistent model requires only specifications of external sources as solar EUV and UV fluxes, aurora particle precipitation, ionospheric convection pattern, and the amplitudes and phases of semi-diurnal tides from the lower atmosphere.

The models of the ionospheric plasma density distribution and TEC depend on a number of upper atmospheric and ionospheric parameters, such as the neutral density, neutral wind, neutral and plasma temperatures, plasmaspheric flux, and ion-neutral collision frequencies. In the numerical modeling of the ionosphere, these parameters are generally often only roughly known and can cause significant uncertainties in the model results (Jee et al., 2005). The physical models are also tested for implementation in the ionosphere tomography though a numerical model is often derived to give a close approximation to the full theoretical calculations under all conditions. The physical model can be used to determine the qualitative relationship, but we do not have to rely on the physical model to provide the quantitative dependence for operational use (Fuller-Rowell et al., 2001). The physical models can match empirical models in accuracy provided accurate drivers are available, but their true value comes when combined with data in an optimal way (data assimilative scenario).

3. International Reference Ionosphere

3.1. General

A preliminary set of IRI tables was presented at the 1972 URSI General Assembly (Rawer et al., 1972) and COSPAR Scientific Assembly (Ramakrishnan and Rawer, 1972). Composite ionosonde profiles, incoherent scatter data, and total electron content (TEC) Faraday measurements played a dominant role in establishing this first precursor of an IRI model.

From the beginning the computer-accessibility of the evolving model was established, a foresightedness that paid off in the long run and contributed considerably to the popularity of IRI in the user community. One should keep in mind that those were the days of punched cards,

paper tape, large mainframes and with still a considerable computer illiteracy in the science community. Making the model software accessible in computer-readable form to a wide user community was still a relatively novel approach; for example, CIRA (COSPAR Reference Atmosphere) continued to be presented primarily in the form of published tables until the release of CIRA-86 in the late eighties. The first widely distributed edition of IRI was released in 1978 (IRI-78) as an URSI Special Report (Rawer et al., 1978) and also as ALGOL and FORTRAN computer codes on punched cards and tape.

The IRI task group was established jointly by COSPAR and URSI in the late sixties to develop and improve a standard model of the ionospheric plasma parameters (electron and ion densities, temperatures, and velocities). The model should be primarily based on experimental evidence using all available ground and space data sources; theoretical considerations can be helpful in bridging data gaps and for internal consistency checks. Where discrepancies exist between different data sources, the IRI team should promote critical discussion to establish the reliability of the different data bases. IRI should be updated as new data become available and as old databases are fully evaluated and exploited.

Using the (CCIR, 1983) world maps for the F2 peak parameters foF2 and M(3000)F2, IRI-78 was a major step forward towards a truly global representation of the ionosphere. By incorporating the maps of the Consultative Committee on International Radiopropagation (CCIR) recommended for international use by the International Telecommunication Union (ITU-R) and URSI, the IRI group underlined its support and concern for radio propagation studies and applications. A special URSI working group was established and succeeded in developing a new set of world maps based on a much better extrapolation scheme for the data-sparse ocean regions (Rush et al., 1989). The improved accuracy over the oceans, however, came at the expense of somewhat less accurate maps for the continents. Different from CCIR who decided to stick with its older maps, the IRI model now provides access to both the CCIR and URSI maps, thus allowing users to utilize the superior accuracy of the URSI maps over the oceans.

For their global distribution both maps rely on the modified dip latitude (modip) that was introduced by Rawer (1963) and is defined as $\tan(\text{modip}) = \text{dip}/(\cos(\text{lat}))^{1/2}$ where dip is the magnetic inclination and lat is the geodetic latitude. Modip was found to better organize features of the ionospheric F2 layer parameters than other magnetic coordinates. This is due to the fact that the ionosphere is controlled by both the orientation of the Earth's rotation axis and the configuration of the geomagnetic field. Therefore, its variation depends on both the geographical and geomagnetic latitudes, which is embedded in modip depending on both the magnetic inclination and the geographical latitude. In recent years the IRI group has taken a more active role in the mapping of F2 peak parameters. The cumulative data volume from the worldwide network of ionosondes has increased significantly since the CCIR and URSI models were developed. Oyeyemi et al. (2007) [M(3000)F2], Oyeyemi and McKinnell (2008) [foF2], McKinnell and Oyeyemi (2009, 2010) [foF2] have trained Neural Networks (NN) with all available ionosonde data and find increased accuracy compared to the older models. Their models for M(3000)F2 and foF2 are now planned for inclusion in IRI as new options. The propagation factor M(3000)F2 is the MUF divided by foF2, where MUF is defined as the highest frequency at which a radio wave can propagate from a given point over a distance of 3000 km. M(3000)F2 can be deduced from vertical-incidence ionograms by the use of standard methods and global spherical harmonics models similar to the foF2 models were developed for M(3000)F2 under the auspices of CCIR and ITU. M(3000)F2 is closely correlated with the F2

peak height, hmF2, and empirical relationships have been developed that describe this dependencies (Dudeney, 1974; Bilitza et al., 1979). The Bilitza et al (1979) formula is used in IRI because it showed best agreement with ionosonde as well as incoherent scatter measurements.

Guided by the knowledge gained from previous data analysis, and from simulations with a physically-based model (Rodger et al., 1989), observations of the F-region critical frequency foF2 (related with the peak electron density NmF2) from all available sites and from many storms were selected by Fuller-Rowell et al. (2000) sorted as a function of local time, season and magnetic latitude, and by the magnitude of the storm as described by the geomagnetic Ap index. Their empirical ionospheric STORM model is incorporated in IRI.and it provides prediction of the dominant ionospheric storm effects on the peak electron density corrected for effects of the planetary geomagnetic 3-hour Ap index from the preceding 39 hours. Relevant empirical model for the storm-time ionosphere peak height hmF2 associated with changes of peak electron density NmF2 has been deduced from the topside sounding database of ISIS1, ISIS2, Intercosmos-19 and Cosmos-1809 satellites which is included in coupled IRI / Plasmasphere code, IRI-Plas (Gulyaeva et al., 2002a,b, 2011; Gulyaeva, 2011a,b).

The structure of the IRI electron density profile is shown in Figure 1 (Bilitza and Rawer, 1990). The electron density profile is divided into eight height regions from the D layer in the lower ionosphere to the topside and the plasmasphere above the F2 peak.

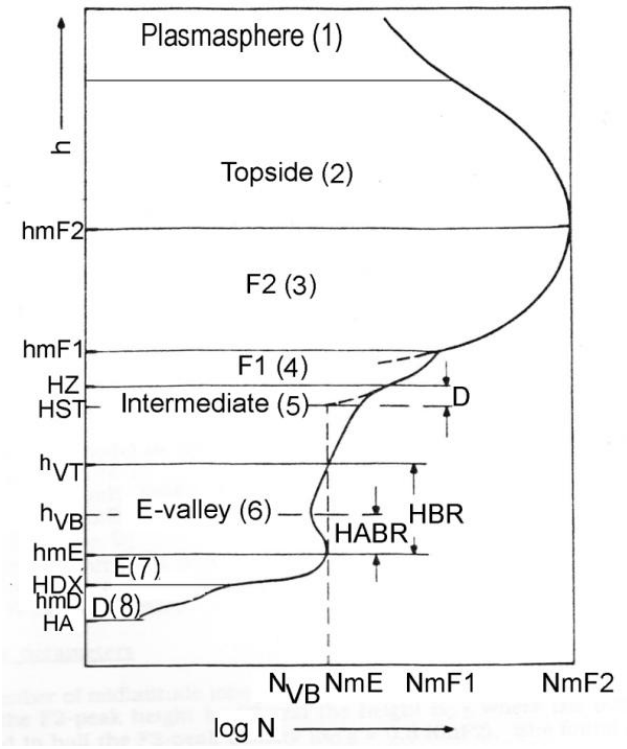

Figure 1. Buildup of IRI electron density profile.

3.2. IRI Topside

By the early seventies the highly successful Alouette 1 and 2 satellites had accumulated a large data base of global topside soundings so that empirical modelling of the topside could be seriously considered. The first major effort was undertaken by Bent and his colleagues (Bent et al., 1972; Llewellyn and Bent, 1973) using more than 50,000 Alouette 1 topside soundings covering the period 1962 to 1966 (low to medium solar activity). For high solar activity they relied on Ariel 3 in-situ measurements for 1967 and 1968 which were combined with F2-peak densities obtained from ground-based ionosondes. Their model is given in graphical form providing plots of the linear variation of their model parameters with daily solar 10.7 cm radio flux (F10.7) for four foF2 classes (2, 5, 8, 11 MHz) and three ranges in geomagnetic latitude (0º to ±30º, ±30º to ±60º, ±60º to ±90º).

In the very first version of IRI (Rawer et al., 1972; Ramakrishnan et al., 1972), topside profiles (range 2 in Figure 1) were based on incoherent scatter data from Malvern (U.K.) and Arecibo (Puerto Rico). The thickness of the upper F-layer was chosen in such a way that the total electron content (TEC) calculated for the IRI profile agreed with TEC measurements. However, the determination of the thickness parameter should really be based on the so-called slab thickness, which is the TEC value normalized with the simultaneously measured F2-peak density. Unfortunately, very little information was available at the time about the global variation of slab thickness. For IRI-1978 Rawer et al. (1978) developed an analytical description of the data base contained in Bent's model using Epstein step- and transition-functions. As in the Bent model the IRI model coefficients are provided as functions of F2 peak plasma frequency (foF2), geomagnetic latitude, and solar activity (F10.7). The analytical representation helped to smooth out some of the unreasonable sharp transitions seen in the original Bent model. An important result of this newer model is a smoothly varying scale height, which is more acceptable than the very irregular scale height behavior obtained with the original Bent model.

As more topside data became available the IRI topside model was evaluated extensively. ISIS 1 and 2, the followon topside sounder satellites to Alouette, were a particular valuable data source (Bilitza et al., 2003). The comparative studies found discrepancies between the data and the IRI model, especially in the upper topside (Iwamoto et al., 2002; Coisson et al., 2002; Bilitza, 2004). Many different profile functions were tested in an effort to improve the IRI model (Bilitza et al., 2006). Simplified aeronomic arguments lead to a Chapman-type profile (Rishbeth and Garriott, 1969)

$$N(h)/NmF2 = \exp\{c[1-z-\exp(-z)]\},\ z = (h-hmF2)/Hm \qquad (1)$$

where NmF2 and hmF2 are the F2 peak density and height, Hm is the Chapman layer topside scale height and c=0.5 or 1 for a Chapman α- or β- function. The α-Chapman scale height Hm is about 3 times less than the topside exponential scale height, Hsc, corresponding to 1/e decay of the peak electron density (Gulyaeva, 2011a).

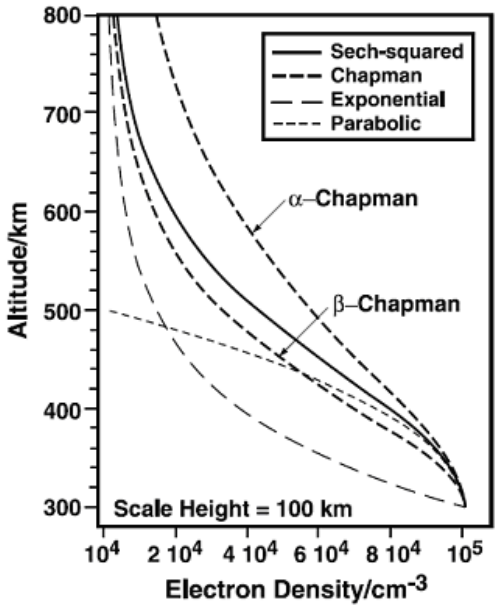

Figure 2. Density profile functions for the topside electron density for a scale height of 100 km (Stankov et al., 2003; reproduced by permission of American Geophysical Union).

Other functions often used in topside modeling include parabolic, exponential, and Epstein-layer (sech-squared) functions (Stankov et al., 2003). Figure 2 shows the typical altitudinal variation behavior of these functions. The Ne-Quick model of Radicella and Leitinger (2001) and Coisson et al. (2006), for example, combined an Epstein F-layer with a height-varying scale height. The merits of different functions in reproducing measured topside profiles and TEC values have been evaluated in a number of studies using different data sources (Stankov et al., 2003; Bilitza et al., 2006; Bilitza, 2009). Stankov et al. (2003), for example, find that average nighttime profiles obtained from AE-C satellite in situ measurements are best represented by the Epstein formulas, whereas the daytime profiles are better approximated by exponential or a Chapman functions. Examples of α-Chapman profile with a constant scale height (dashed curves in Figure 3) demonstrate insufficient plasma density in the topside ionosphere and plasmasphere as compared to full IRI-Plas electron density profile (Gulyaeva et al., 2002a,b).

As a result of these studies two new options were introduced in IRI starting with 2007 version (Bilitza and Reinisch, 2008). The first is a correction factor for the 2001 model based on over 150,000 topside profiles from Alouette 1, 2, and ISIS 1, 2. This term varies with altitude, modified dip latitude, and local time (Bilitza, 2004). The second option is the NeQuick topside model that was developed by Radicella and his collaborators over the last decade (Radicella and Leitinger, 2001; Coisson et al., 2006) using Intercosmos 19 topside sounder data in addition to the ISIS 1 and 2 data. The model fit analytical functions on a set of anchor points, namely the E; F1 and F2 layer peaks, to represent these principal ionospheric layers and compute the electron density profile. NeQuick is adopted by the ITU-R recommendation for TEC modeling (Hochegger et al., 2000).

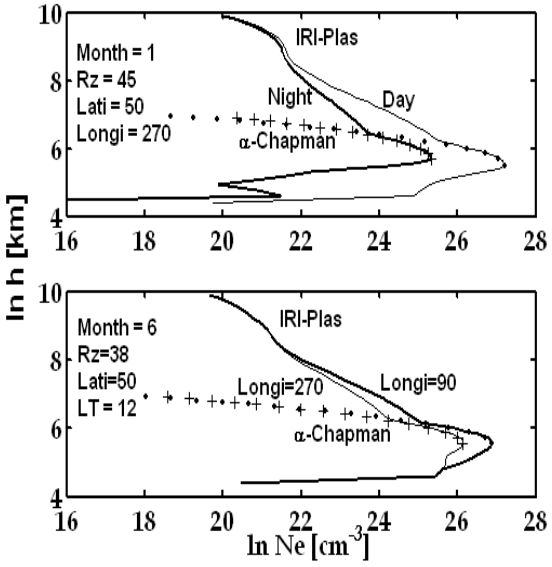

Figure 3. The IRI-Plas model electron density profile in comparison with α-Chapman profile. Noon and midnight examples (upper panel), noon ptofiles at different longitudes (lower panel).

The NeQuick model is divided into two regions: the bottomside, up to the F2-layer peak, consists of a sum of five semi-Epstein layers-1 (Rawer, 1984; 1991) and the topside is described by means of an only sixth semi-Epstein layer with a height-dependent thickness parameter, and in this way produces a smooth transition from an atomic oxygen ionosphere near the F-peak to a light ion ionosphere higher up. The implementation of NeQuick topside into IRI is the only part of IRI model which requires the use of M(3000)F2 in addition to foF2 and hmF2 values. This parameter can be computed either from the CCIR model or inverting the IRI formula that provides hmF2 in terms of M(3000)F2 (Bilitza et al., 1979).

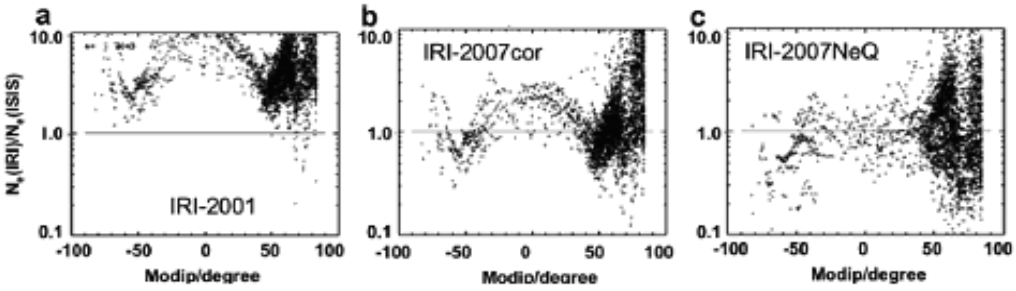

Figure 4. (a–c) Ratio of ISIS-2 topside sounder data versus model predictions at 1000 (±50) km above the F2 peak using IRI-2001 (a), IRI-2007-cor (b), and IRI-2007-NeQ (c). The total number of data points is n = 3043 (Bilitza, 2009; reproduced by permission of Elsevier).

Figure 4 shows the model-data ratio for the three IRI topside options (IRI-2001, IRI-2001 corrected, IRI-NeQuick) at 1000 km altitude using ISIS-2 sounder measurements. A significant improvement (values closer to 1) is achieved with the inclusion of the correction term and even more so with the NeQuick option. The results for all available ISIS 1 and 2

data are summarized in Table 1 indicating a factor of 4 improvement when using the correction term and a factor 7 improvement with the NeQuick model.

Two recent modeling activities promise future improvements for the representation of topside electron density profiles in IRI. Reinisch et al (2007) have developed the Vary-Chap approach. While the standard Chapman profile function (Eq 1) is deduced for a single constituent gas with a constant scale height, Reinisch et al. (2007) have determined the profile function for a more realistic multi-constituent case with height-varying scale height expanding on earlier work by Rishbeth and Garriott (1969). Figure 5 shows how well this new function represents an ISIS-2 topside sounder profile.

Table 1. Mean and standard deviation of the percentage difference between the IRI model and ISIS-2 topside sounder data using 7 separate Alouette/ISIS data sets and all three options available in IRI-2007: IRI-2001 [IRI], corrected IRI-2001 [cor], NeQuick [NeQ] (Bilitza, 2009; reproduced by permission of Elsevier)

		ISIS-2	ISIS-1	Alouette -2	Alouette-1u	Alouette-1t	Alouette-1p	All
IRI	**Std**	10.39	7.44	9.90	4.50	1.83	2.73	
	Mean	-2.12	-1.79	-2.23	-0.50	-0.58	-1.01	-1.65
Cor	**Std**	2.97	2.72	2.04	2.44	1.11	1.55	
	Mean	-0.61	-0.43	-0.38	-0.22	-0.25	-0.41	-0.46
NeQ	**Std**	1.92	1.74	0.98	1.96	1.04	1.48	
	Mean	-0.31	-0.21	-0.04	-0.11	-0.20	-0.36	-0.24
	n	25,214	20,105	5166	19,434	37,240	12,900	120,059

IRI = IRI-2001, cor = IRI-2007-corrected, NeQ = IRI-2007-NeQ.
n – number of profiles, All – all 6 data sets together.

Gulyaeva's (2003) modeling efforts have focused on the topside half-density point, h0.5top. This is the height where the topside electron density has dropped down to half the F2 peak density, a point that can be easily scaled from topside profiles. The ISIS1, ISIS2 and IK19 topside sounder profiles were used to develop a model for h0.5top in terms of sunspot number, local time, and geomagnetic latitude. This model, IRI-Plas, uses a coefficient, 'q-factor', which serves for a correction of the IRI-2001 topside model forcing it to fit the h0.5top parameter (Gulyaeva et al., 2002a,b; Gulyaeva and Titheridge, 2006).

Comparisons of IRI-Plas and NeQuick with Topex-TEC measurements are plotted in Figure 6. The dual-frequency altimeters on board the Topex/Poseidon (T/P) and Jason satellites can provide the ionospheric electron content (TEC) over the oceans for altitudes ranging from 65 to 1336 km (Fu et al., 1994). TEC-model is calculated from the bottom of ionosphere to the TOPEX orbit altitude of 1336 km (Gulyaeva et al., 2009). Figures 6a and b show the diurnal/seasonal variation of TEC as measured by Topex and as given by the models for high solar activity (2002) and low solar activity (2007), respectively. All model results are obtained with CCIR peak maps, and Topex TEC are averaged for each hour ±0.5 h, within longitude/latitude bins in step of 5º and compiled/averaged for each month/season. The models are capable of reproducing the main variations of the Topex TEC but in the worst case depart from the observations up to 20 TECU (TEC unit, TECU=10^{16}el/m^3).

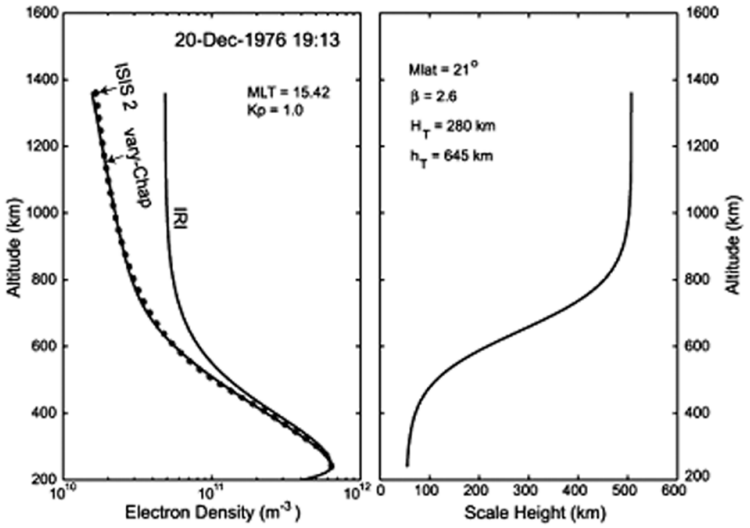

Figure 5. The vary-Chap function (solid line) closely matches the measured ISIS 2 profile (dots); the IRI profile largely overestimates the densities at higher altitudes. The right panel shows the corresponding scale height function H(h) showing a clear transition from an O^+ to an H^+ ion gas higher up (Reinisch et al., 2007; reproduced by permission of Elsevier).

A particular challenge in modeling the topside electron density profile is the accurate representation of the fountain effect at equatorial latitudes. At F-region heights this effect produces the well-known crests at about 18 degrees dip latitude on each side of the magnetic equator (equator anomaly, EA) and a relative minimum at the magnetic equator. With increasing height the two latitudinal peaks move closer towards the magnetic equator and merge into a single peak at the magnetic equator at a height of about 1000 km (Bilitza et al., 2006). Almost all topside models are normalized to the F2 peak density, NmF2. Models for NmF2 are well established and provide the typical camelback signature of the equator anomaly. To reach a single equatorial peak at high altitudes, the topside profile function therefore has to counterbalance the EA signature imprinted by the NmF2 model. An improved representation of the IRI topside electron density profile is also a necessary step towards a successful merging of the ionosphere and plasmasphere models because plasmaspheric models often use the IRI topside density at a certain fixed height as a footpoint for their model.

Figure 7 illustrates the representation of the EA region as it is given by the four options available in IRI for the topside electron density (a – IRI-2001, b – IRI-corr., c – IRI-NeQuick, d – IRI-Plas). The contour plots show the distribution of ionization with geomagnetic latitude and height. At F-region altitudes the models are very similar with the two maxima at about 15 degrees and with the neutral wind pushing ionization up the field line in the northern (summer) hemisphere and down the field line in the southern (winter) hemisphere resulting in the hemispheric asymmetry in F-peak height. However, drastic differences appear between the four options with growing altitudes. The IRI-corr model (Figure 7b) and IRI-Plas model (Figure 7d) produce the expected merging of the EA double peak into a single peak at higher altitudes while the other two models exhibit unrealistic features: IRI-2001 (Figure 7a) shows almost vertical profiles, and IRI-NeQuick (Figure 7c) shows still separate EA peaks at high altitudes.

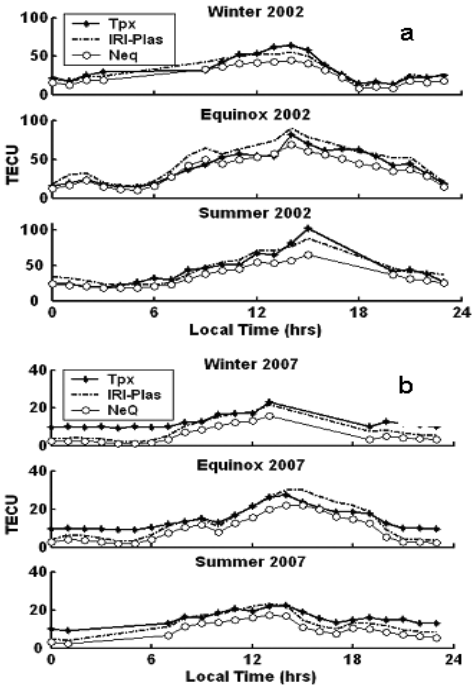

Figure 6. Seasonal-diurnal variation of TEC-model (IRI-Plas and NeQuick) compared with Topex data: (a) high solar activity (2002); (b) low solar activity (2007).

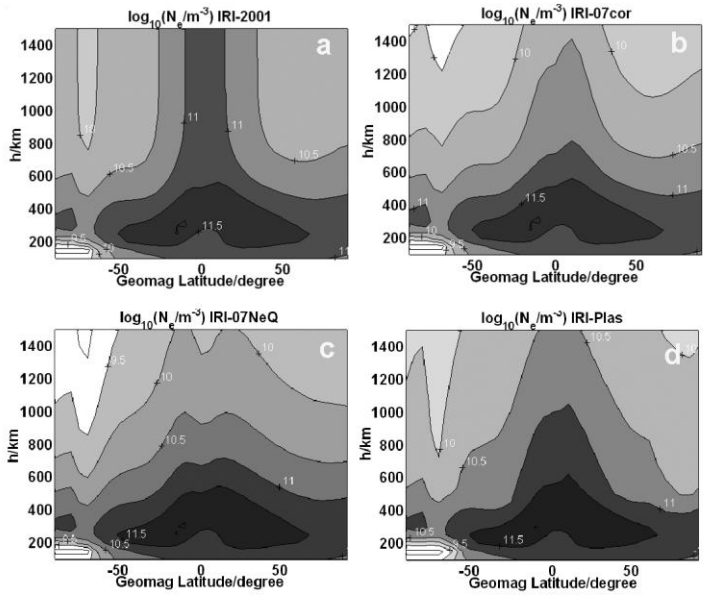

Figure 7. (a–d) Geomagnetic latitude versus height contour plot of the logarithm of electron density at Longitude = 0 and Universal Time (UT) = 16:00 for medium solar activity (R12 = 50) and northern summer for the different IRI model options: IRI-2001 (a), IRI-2007-cor (b), IRI-2007-NeQ (c) and IRI-Plas (d). The increment between contour lines is 0.5 starting from 11.5 (black) down to 9.5 (white).

3.3. IRI Bottomside

The bottomside of the F2 region (range 3 in Figure 1) is represented by the function

$$N(h) = NmF2*\exp(-x^{B1}) /\cosh(x) \quad (2)$$

where

$$x = (hmF2-h)/Bo$$

and B0 and B1 are profile parameters that describe the thickness and shape of the bottomside layer. This function was proposed by Ramakrishnan and Rawer (1972) who found that with it they could closely reproduce a set of representative profiles obtained from ionosonde measurements. For B0 two model options are offered in IRI. The standard Table option is based on a table of values that was assembled for different latitudes, times of day, levels of solar activity, and seasons (Bilitza et al., 2000).

The second option is based on work by (Gulyaeva (1987; 2007) and therefore is called the "Gulyaeva" option. Gulyaeva (1987, 2007) found a close correlation between the F2 peak height hmF2 and the height $h_{0.5}$ where the electron density has decreased to half the F2 peak density, $N_{0.5}$ = 0.5 NmF2 This relation in a function of the solar zenith angle and season. The shape parameter B_1 is fairly constant and shows only significant differences from day to night. The typical daytime value is 1.9 and the nighttime value is 2.6. Epstein step functions are used to model the day-night transitions at dawn and dusk. Both model options, however, are based on a relatively small data base and have shown shortcomings in comparisons with ionosonde and incoherent scatter data. Altadill et al. (2008, 2009) have applied spherical harmonics analysis to data from 27 globally distributed ionosonde stations obtaining new models for B_0 and B_1 that more accurately describes the observed variations with latitude, local time, month, and sunspot number. Overall the improvements over the IRI-2007 model options are of the order of 15 to 35%. The largest improvements are seen at low latitudes. This new model will be included in IRI-2011 as a third option.

A parabolic F1 layer is included in the bottomside electron density profile when the NmF1 model (Ducharme et al., 1973) predicts the existence of this layer. If no F1 feature is predicted (e.g. at night) the F region is represented b a single F2 layer. The F1 layer (range 4 in Figure 1) starts from the F1 layer peak height, hmF1, where the bottomside profile reaches the F1 peak density, NmF1. The models for NmF1 and for the F1 layer thickness C_1 were developed based on ionosonde data.

While in the F region the IRI electron density profile is normalized to the F peak density and height, it is normalized to the E region peak density and height in the E region. A merging algorithm is used to join the two profile parts. This transition region extends from the top of the E valley to the bottom of the Fl layer (range 5 in Figure 1). In the intermediate region the bottomside profile is merged parabolically with the E-F valley profile. First, the height HST is found where the bottomside profile density is equal to the E peak density NmE. Starting from a point HZ slightly above HST, the profile is then bent downwards so that it meets the vally top. The valley between the E and F regions (range 6 in Figure 1) is derived mostly from the incoherent scatter radar data since it is unvisible with the vertical sounding of the ionosphere. Analytical expressions are used to describe the variation of the valley parameters (depth and width) with solar zenith angle and latitude (Gulyaeva, 1987). The

valley marks the region between the E and F layers and reaches great depth at nighttime due to the fast recombination of electrons and ions but it is narrow for the daytime.

The current formalism could lead to discontinuities or artificial valleys under conditions when merging was particularly difficult to accomplish, because of large differences between E and F peak densities and/or small differences between the E and F peak heights. A better functional description for the merging region was developed by Reinisch and Huang (1999). The new algorithm overcomes these problems and provides a much better representation of profile shape observed by ionosondes.

The E region is the region of peak ion/electron production, and the electron distribution is largely controlled by the solar zenith angle. The E-peak height is remarkably constant, and is typically found at about 110 km. The E- peak density, NmE, is about an order of magnitude lower than the F2-peak density. Kouris and Muggleton (1973) developed a model for NmE based on ionosonde data from representative low and middle latitude stations. In addition to the solar zenith angle dependence the model describes the variation with solar activity, season, and geographic latitude. The model was adopted for radiowave propagation applications by CCIR. For IRI the model was improved for large solar zenith angles (nighttime) with the help of incoherent scatter radar results (Bilitza and Rawer, 1990). The off-equator E region electron density enhancements are found to be closely connected with the bottomside of the F region equatorial anomaly crests, where the component of the electron density parallel to the magnetic field line is maximum (Chu et al., 2009). It appears that the off-equator E region electron density enhancements are very likely the footprints of the F region equatorial anomaly crests.

The IRI generally describes the E-region electron density (range **7** in Figure 1) well, but the ionization enhancement at auroral latitudes caused by precipitating particles has not been provided till recently. One of the new features in IRI-2007 (Bilitza and Reinisch, 2008) is a Neural Network (NN) model for this auroral region that was trained with a large volume of EISCAT incoherent scatter data (~700,000 data points) and also with 115 profiles obtained from rocket borne wave propagation experiments (McKinnell et al., 2004; McKinnel and Friedrich, 2006). The model describes the density variations in terms of local magnetic time, riometer absorption, local magnetic index K, solar zenith angle, and atmospheric pressure, the latter accounts for variations with height and season. Newer efforts by Fernandez et al. (2010) and Zhang et al. (2010) using TIMED SABER and GUVI data, respectively, promise major improvements in the representation of the high latitude E region in IRI. As a result of the modeling work with GUVI data by Zhang et al. (2010) the next version of IRI will for the first time include a representation of auroral boundaries and their movement with magnetic activity.

The lower ionosphere is defined below the D region peak density NmD and height hmD. The D region (range 8 in Figure 1) is characterized by large variability and a very small database for modeling studies. The only data sources are rocket experiments, because the region is too low for satellites and the densities are too low for ground ionosondes and radars. IRI includes three options for the description of D region electron densities, thus reflecting the large uncertainties that still exist in this region. Option 1 is the current D region model that was developed by Mechtley and Bilitza (1974) on the basis of a rather limited set of representative rocket data.

Option 2 is the FIRI model by Friedrich and Torkar (2001) derived from a database of the most reliable D region rocket measurements (-200 profiles) collected by these authors

(Friedrich et al., 2001). They experimented with different modeling approaches, including the strong dependence on solar zenith angle and considering to various degrees dependencies on season, latitude, solar activity, and neutral density and even an extension to high latitudes. Their most recent modeling concept combines the rocket data with the results of a theoretical model. The FIRI model is given as a table of values and model profiles are obtained by suitably interpolating using the user-specified zenith angle, latitude, season, and solar activity.

Option 3 is the model of Danilov et al. (1995) based primarily on Russian rocket data. In addition to the dependence on solar zenith angle, latitude, and solar activity it also provides users with an estimate of the changes observed in the D region during disturbed conditions for winter daytime. Although their rocket database is quite limited in volume, they find that the data can be grouped into five distinct classes using the following criteria: (1) undisturbed conditions, (2) weak winter anomaly (WA) defined by an increase of the absorption in the 2-2.8 MHz range at short A3 paths by 15 dB, (3) strong WA defined by an increase of 30 dB, (4) weak stratospheric warming conditions defined by a temperature increase at the 30 hPa level by 10 degmes, and (5) strong stratospheric warming conditions defined by an increase of 20 degrees.

Thus, the IRI electron density profile below the F2 peak is determined from the key parameters:

Peak densities: NmD, NmE, NmF1, NmF2
Peak heights: hmD, hmE, hmF1, hmF2
Layer thickness: Bo, B_1, C_1
Valley parameters: h_{VT}, h_{VB}, N_{VT}

3.4. Additional IRI Parameters

For many applications of ionospheric models the single most important parameter is the electron density and in particular the electron content along a radio wave signal path. But with the increased utilization of space other parameters have become of importance as well. The IRI model includes specifications for many of these parameters including the percentages of the major ions (also called ion composition), the temperatures of electrons and ions, the ion drift at the magnetic equator that is important for the development of the Equatorial Ionization Anomaly, and the occurrence probability for spread-F a phenomena that can cause havoc to communications and navigation primarily at low latitudes.

The ion composition models in IRI are based mostly on rocket measurements in the bottomside ionosphere and on satellite measurements in the topside ionosphere. Incoherent scatter radar measurements have been used to evaluate and improve these models. The dominant ion in the F region is O^+, at higher altitudes light ions, mostly H^+ with some He^+ and N^+, become more important and than dominant. Towards lower altitudes the percentage of molecular ions, $O2^+$ and NO^+ increases and they become the dominant constituent in the E region (100-150 km). Even lower down, in the relatively dense D-region (~80-90 km) Cluster ions can form and make up most of the ion population. For the topside IRI relies on the modeling work of Triskova et al. (2003) and Truhlik et al. (2004) who have compiled a large data base of satellite ion data (AE-C, -D, -E, Interkosmos 24, ISIS-2, ISS-b) and analyzed these data to establish the dominant global and temporal variation patterns.

The ion composition in the bottomside is the result of modeling work by Danilov and Smirnova (1995) who used their compilation of Russian rocket data together with data from the AE-C, S3-1, AEROS-B, Sputnik-3 and Cosmos-274 satellites. As a second option IRI also offers the earlier models by Danilov and Semenov (1978) for the bottomside and Danilov and Yaichnikov (1985) for the topside. All of these models describe variations with altitude, latitude, solar zenith angle, season, and solar activity. Discrepancies were found when using IRI molecular densities to compute airglow and EUV response (Nicolls et al., 2006; Vlasov et al., 2010). To overcome these problems Richards et al. (2010) proposed a new bottomside model for IRI that is based on the well established photochemistry in this region using the FLIP (Richards, 2002) and NRLMSIS00 (Picone et al., 2002) models and normalizing the outcome to the IRI electron density profile. The Richards et al. (2010) model will be introduced in IRI as a new option for the bottomside ion composition.

Electron temperature (T_e) and ion temperature (T_i) have been measured by incoherent scatter radars (ISRs) from the ground and insitu by satellite experiments. Satellite data provide the global morphology of temperature variations and the ISRs are the ideally resource for studying diurnal, seasonal, and solar cycle variations. A first global representation of T_e and T_i for IRI was developed by Bilitza (1981) based on a combination of satellite and ISR data. More recently Truhlik et al. (2000) have develop a model based on their large satellite data base. Both models describe variations with altitude, dip latitude, and magnetic local time and both models are given as separate options in IRI. A recent extension of the Truhlik et al (2000) model now also includes the dependence on the F10.7 solar flux based on work by Bilitza et al. (2007) and Truhlik et al. (2009) using satellite data and comparisons with the theoretical FLIP model and the empirical ISR model of Zhang et al. (2005). Like for T_e the global representation of T_i relies heavily on satellite data (Bilitza, 1981). Below 120 km thermal equilibrium is assumed and both plasma temperatures coincide with the neutral temperature as given by the NRLMSIS00 model (Picone et al., 2002). Higher up the heating of the electron gas through photo-electrons keeps T_e above T_i and the transfer of energy from the electrons to the ions through Coulomb collisions keeps T_i above T_n. For these reasons IRI enforces $T_e \geq T_i \geq T_n$ throughout the ionosphere.

3.5. IRI Plasmasphere Extension

An increasing number of users of ionospheric models also require information about the plasma conditions above the ionosphere in the plasmasphere (region 1 in Figure 1). The plasmasphere is the region from the top of the ionosphere up to a boundary, the plasmapause, where a sharp drop in plasma density occurs. The plasmasphere is a torus of relatively cold (~1-50 eV) and relatively dense (> 10 cm^{-3}) plasma that consists mostly of H^+ ions trapped along Earth's magnetic field lines and thus co-rotating with Earth. The plasmasphere structure and dynamics are driven by ionospheric sources and the plasmasphere feeds back the ionosphere by night and during the post-storm recovery. The Global Positioning System (GPS) receivers measure the total electron content through the ionosphere and plasmasphere so any use of GPS data needs to account for the plasmaspheric contribution to the total electron content between ground station and satellite (Yizengaw et al., 2007)..Low-earth orbit measurements include the upper reaches of the

ionosphere and the thermosphere, which must be correctly modeled in order that the measurements properly constrain the outer plasmasphere (e.g. Heise et al., 2002).

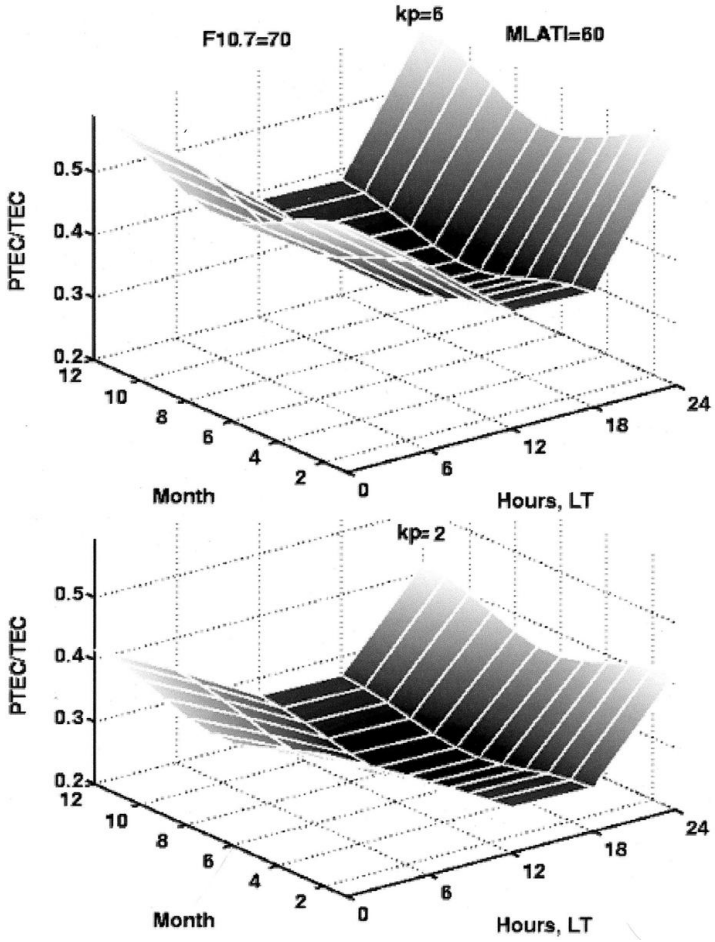

Figure 8. Seasonal/local time variation of plasmaspheric contribution to TECgps simulated with IRI-Plas model under quiet magnetic conditions (lower panel) and disturbed conditions (upper panel).

These TEC measurements can be used directly or organized into two-dimensional 2D TEC maps to infer information on the horizontal structuring of the electron density. However, information on how plasma can be lifted to high altitudes and transported to other regions, polar outflow, and other vertical dynamical changes is lost with such simple mapping algorithms. In order to obtain information on the vertical structure of the electron density, its temporal variation, and transport, 4D model is necessary. For the point profiles, measured by ionosondes or incoherent scatter radars (ISR), there is no information about large-scale horizontal gradients and convection of plasma that causes structuring at the profile position. The time-evolving nature of 4D modeling is crucial due to temporal and spatial changes of electron density distribution within a given region.

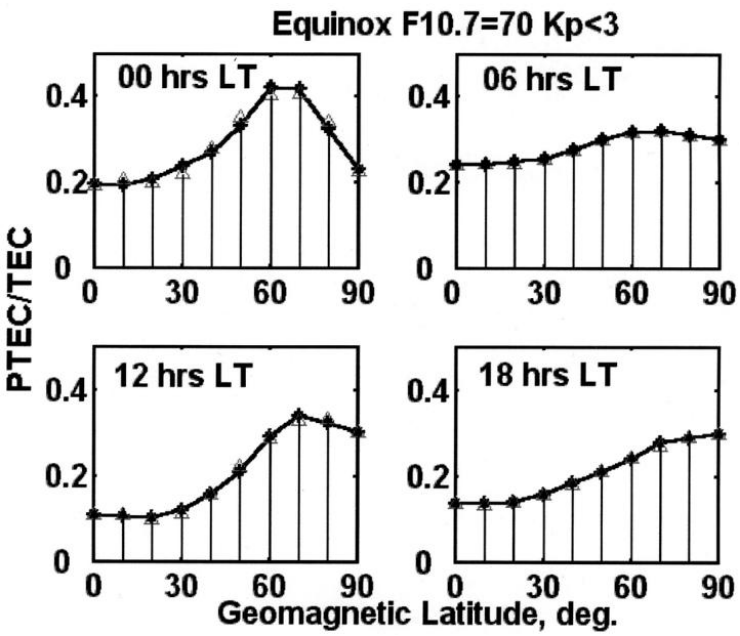

Figure 9. Plasmasphere contribution to TECgps varying with magnetic latitude simulated with IRI-Plas model during equinox under quiet magnetic conditions at low solar activity.

For IRI serving as a background model for tomographic reconstruction of 4D plasma structure from GPS-derived TEC, the IRI topside profile should be extended towards few Earth's radii (Bust and Mitchell, 2007). Figure 8 provides hints on plasmasphere contribution in GPS-derived TEC. Ratio of plasmaspheric electron content, PTEC, to the TEC (from the ground surface to 20,200 km at the GPS orbit) at sub-auroral latutude can comprise 40% towards midnight under quiet magnetosphere (bottom section, kp=2) and can exceed 50% during magnetic storm (upper section, kp=5). The diurnal variation of PTEC/TEC is illustrated for four selected local times in Figure 9 where this ratio is plotted versus modified dip latitude (modip).

A number of approaches have been proposed for extending IRI to plasamspheric altitudes. We will discuss briefly four of these models.

The **Global Core Plasma Model (GCPM-2000)** of Gallagher et al. (2000) is an empirical description of thermal plasma densities in the plasmasphere, plasmapause, magnetospheric trough, and polar cap. It has been developed from retarding ion mass spectrometer data collected by the Dynamic Explorer satellite, includes several previously published regional models, and represents the low energy plasma distribution along the field lines from 0 to 24 hours magnetic local time world-wide. GCPM-2000 is smoothly coupled to IRI in the transition region of 400-600 km altitude. It was applied also for the plasmasphere extension of NeQuick model (Cueto et al., 2006).

The **Global Plasmasphere Ionosphere Density (GPID)** model is a semi-empirical representation that was developed by Webb and Essex (2000, 2004). GPID includes IRI below about 500 km to 600 km and extends with a theoretical plasmasphere electron density description along the magnetic field lines. Authors report on drawbacks of merging of the IRI with the plasmasphere part of GPID.

The **IMAGE/RPI plasmasphere model** (Huang et al., 2004) is based on radio plasma imager (RPI) (Reinisch et al., 2000) measurements of the electron density distribution along magnetic field lines. A plasmaspheric model is evolving for up to about four earth radii. The depletion and refilling of the plasmasphere during and after magnetic storms is described in Reinisch et al (2004). A power profile model as function of magnetic activity was developed from RPI observations for the polar cap region (Nsumei et al., 2003).

Table 2. List of IRI-Plas model output parameters

Symbol	Designation
Year	Year
MN	Month
DY	Day of month
UT	Universal time (h)
LT	Local time (h)
MLT	Magnetic local time (h)
XHI	Solar zenith angle (º)
Rz	Sunspot number
Cov	Solar radio flux F10.7 (Covington index)
Kp	Planetary geomagnetic index, Kp
GLAT	Geodetic latitude (º)
GLON	Geodetic longitude (º)
MLAT	Geomagnetic latitude (º)
MLON	Geomagnetic longitude (º)
MODIP	Modified Dip latitude (º)
foF2	The F2 layer critical frequency (MHz)
hmF2	The F2 layer peak height (km)
NmF2	Peak electron density (m^{-3})
h05bot	Bottomside half peak density height (km) at Ne=0.5 NmF2
h05top	Topside half peak density height (km) at Ne = 0.5 NmF2
Nes	Electron density at O^+/N^+ transition height (m^{-3})
Nepl	Electron density at 20,200 km (m^{-3})
ECbot	Electron content from 65 km to hmF2 (TECU)
ECtop	Electron content from hmF2 to 1364 km, Topex orbit (TECU)
ECpl	Electron content from 1364 to 20,200 km (TECU)
TEC	Total electron content from 65 to 20,200 km, GPS orbit (TECU)
TAU	Slab-thickness, km (TEC/NmF2)
Hsc	Topside exponential scale height (km)
h	Altitude over the Earth (km)
Ne	Electron density at altitude h (m^{-3})
Te	Electron temperature at altitude h (ºK)
Ti	Ion temperature at altitude h (ºK)
Tn	Neutral temperature at altitude h (ºK)

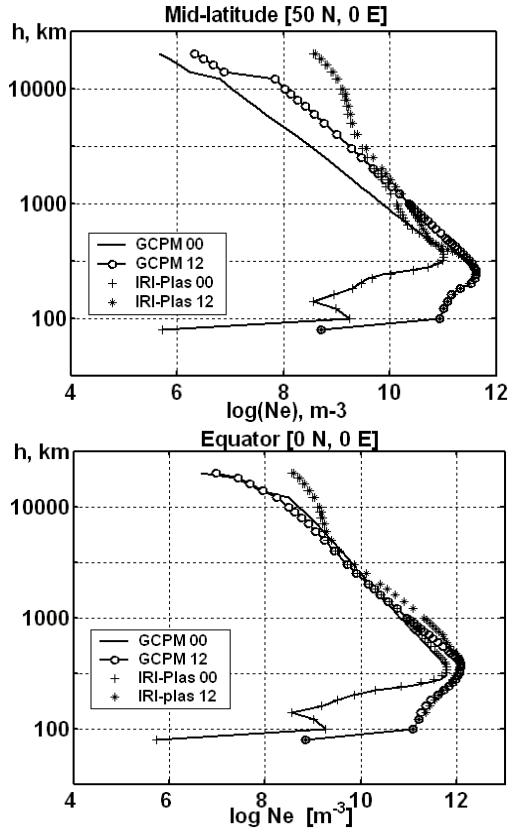

Figure 10. Comparison of GCPM and IRI-Plas plasmasphere electron density profile for noon and midnight: (a) mid-latitude; (b) megnetic equator.

The **IZMIRAN plasmasphere model** (Chasovitin et al., 1998; Gulyaeva et al., 2002a,b) is an empirical model based on whistler and satellite observations. IZMIRAN is the Institute of Terrestrial Magnetism, Ionosphere and Radiowaves Propagation. The IZMIRAN plasmasphere model presents global vertical analytical profiles of electron density (Ne) smoothly linked with the IRI electron density profile at altitude of one basis scale height above the F2 peak (400 km for electron temperature) and extended towards the plasmapause up to 36,000 km (IRI-Plas). For the smooth fitting of the two models, the shape of the IRI topside electron density profile was changed based on ISIS 1, ISIS 2 and IK19 satellite inputs (Gulyaeva 2003). ISIS is the International Satellites for Ionospheric Studies satellite program and IK-19 is the abbreviation for the Russian Intercosmos-19 satellite. The plasmasphere model depends on solar activity and magnetic activity (kp-index). List of IRI-Plas output parameters is given in Table 2. Figures 8 and 9 presents results of calculations with IRI-Plas model (Gulyaeva et al., 2002a,b) which are consistent with observations (Gulyaeva and Gallagher, 2007).

In order to evaluate a measure of the plasmasphere contribution to the transionospheric-transplasmaspheric TEC, two plasmaspheric extensions of the International Reference Ionosphere model, IRI-Plas (IRI-IZMIRAN) and IRI-GCPM, are compared (Gulyaeva and Gallagher, 2007). The both models differ from the original IRI electron density height distribution in the topside ionosphere. The GCPM algorithm includes a search for the best

fitting transition height between the ionosphere and plasmasphere, which is usually found at altitudes of 400 to 600 km depending on location and conditions. The model of the IRI-Plas topside profile semi-thickness, equal to the altitude range from the ionosphere peak height to the topside half peak density height, in terms of geomagnetic latitude, diurnal, seasonal, and solar cycle variations has been included in the IRI-Plas code (Gulyaeva, 2003; Gulyaeva and Titheridge, 2006). Further improvement to the analytical adjustment of the IRI topside profile to the half peak density point has been made by incorporation of TECgps input in data assimilative mode of operation updating three model parameters: (1) an instantaneous peak electron density (Gulyaeva et al., 2011); (2) an instantaneous F2 layer peak height (Gulyaeva, 2011b); (3) the electron density scale height at the lower topside (Gulyaeva, 2011a).

Comparison of IRI-Plas and GCPM electron density profiles near magnetic equator and middle latitude at low solar activity and quiet magnetic conditions is shown in Figure 10a,b for noon and midnight. The IRI part in the bottomside and the lower topside coincide in the both models fitted to CCIR (ITU-R) F2 peak predictions. The plasma density at 20,000 km is coincident for day and night with IRI-Plas and GCPM near the magnetic equator, they are slightly different with GCPM at mid-latitude but they differ up to the order of magnitude of the absolute values near the GPS orbit in two models. With more plasmasphere modeling these differences could be resolved (Jorgensen, 2010).

Both GCPM and IRI-Plas are statistical models derived from many years of measurements designed to represent typical conditions as a function of geomagnetic and solar activity. Much like a weather forecast, these are not capable of always representing dynamically driven conditions at any given time. To the extend that TEC and new satellite measurements are accumulated into a statistical quantification of plasma densities at differing solar and geomagnetic conditions, a more meaningful comparison can be made to a statistical model.

Data assimilation procedures are extensively being developed for near real time forecasting of the ionospheric weather. They are organized by merging, by any means, a model which is a physical description or an empirical (analytical) description of a system with measurements which constrain the state or evolution of the system in some relevant way. The free model parameters are then adjusted to maximize the agreement between the model and the measurements. Final product of the ionosphere/plasmasphere standard model would be incomplete if it could not provide guidance on quantitative measure of the ionospheric weather ranging from quiet conditions to severe storm in the ionosphere and plasmasphere. Such specification is proposed in the next Section.

4. Ionospheric Weather Indices

The short-term perturbations of the ionospheric parameters vary from a few seconds to a few hours, induced by the solar flares, the solar wind, the coronal mass ejection, affecting the Earth's magnetosphere, plasmasphere and ionosphere. Apart from the monthly average variations provided by IRI-Plas model, the daily assessment and forecast of the ionosphere variability are required for many applications (Jakowski et al., 2006). The negative or positive percentage deviation of the current value of foF2 from the quiet background value can serve as an "ionospheric activity", AI, index, characterizing a measure of the ionosphere disturbance (Kutiev and Muchtarov, 2001; Bremer et al., 2006). So defined index, however,

does not provide a uniform measure of negative and positive phases of the ionospheric storm, because positive deviations are deeper than negative ones (Kouris et al., 1999). In particular, the depletion of the peak electron density cannot reach 100%, because a decrease in foF2 to zero would imply an annihilation of the ionosphere. On the other hand, there is no limit imposed on an increase in foF2 during the positive phase of the ionospheric storm when the critical frequency could exceed the median value by a few hundreds of percent.

To avoid these disproportions the decimal logarithm of the hourly value of NmF2 (or TEC), normalized by the quiet reference (median), NqF2 (or TECq), is taken as a measure of the NmF2 (or TEC) variability (Gulyaeva, 1996, 2002c; Field and Rishbeth, 1997; Fuller-Rowell et al., 2001; Gulyaeva et al., 2008). For the quiet reference, 27 days (solar rotation) daily-hourly median of foF2 or TECgps can be taken from the observations, or IRI-CCIR (ITU-R) predictions can serve as a reference.

The logarithmic scale of the deviations is presented as a decimal logarithm of the ratio of the current hourly value of NmF2 (TEC) to the quiet background values NqF2 (TECq):

$$DNmF2 = \log(NmF2/NqF2) \quad (3a)$$

$$DTEC = \log(TEC/TECq) \quad (3b)$$

The sign of DNmF2 (DTEC) specifies the positive or negative phase of the ionospheric perturbation. We assume that the period of 27 days corresponding to the solar rotation yields median values that might also be valid for day 28. This appears to be a reasonable solution for the forecasting purposes, since one has a reference value one day in advance as distinct from the monthly median available only after the month has passed.

For indexing the ionosphere variability similar to geomagnetic k-indices (Menveielle and Berthelier, 1991) we introduce the ionospheric weather index W with thresholds specified in Table 3. We use a non-uniform logarithmic scale similar to Gulyaeva (1996). The intervals for the positive and negative deviation of (Eq. 3a,b) are equal to each other but the relevant threshold of the changes in NmF2 or TEC would be different for the negative and positive deviations. Index W=±1 is used for the quiet state, W=±2 for the moderate disturbance, W=±3 for the moderate ionospheric storm or sub-storm, and W=±4 for the intense ionosphere storm. Criteria for selection of such intervals are based on the conventional evaluation of the negative ionospheric NmF2 deviation within [0, −10%] from the quiet reference for the quiet state, [−10, −30%] for the moderate disturbance, [−30, −50%] for the moderate ionospheric storm, and a depletion of NmF2 greater than −50% for the intense storm conditions. It is found that the moderate disturbance (W = ±2) is a prevailing state of the ionospheric weather. The stormy conditions comprise 1 to 20% of times which occur more frequently at high latitudes, by night, during equinox and winter.

Example of W index inferred from GPS-TEC global ionospheric map, GIM, at solar maximum on 15-17 July 2000 (Figure 11) demonstrates electron content depletion (upper panel) at grid point in the Northern hemisphere [50ºN, 0ºE] but positive storm effect (TEC enhancement) at the magnetic conjugate point [42ºS, 19ºE] (middle panel) in the Southern hemisphere. The W index reached storm peak at the main phase of magnetosphere storm, registered with Disturbance Storm Time, Dst, index (lower panel).

Table 3. Ionospheric weather index W, relevant thresholds of logarithmic deviations (X=NmF2 or X=TEC, Xq - quiet reference) and corresponding state of the ionosphere

W	DN=log(X/Xq)	State
4	DN > 0.301	Intense positive W^+ storm
3	0.155<DN≤0.301	Moderate W^+ storm or W^+ sub-storm
2	0.046<DN≤0.155	Weak W^+ disturbance
1	0.0<DN≤0.046	Quiet W^+ state
-1	-0.046≤DN<0.0	Quiet W^- state
-2	-0.155≤DN<-0.046	Weak W^- disturbance
-3	-0.301≤DN<-0.155	Moderate W^- storm or W^- sub-storm
-4	DN<-0.301	Intense negative W^- storm

Taking advantage of availability of worldwide TECgps data in the Global Ionospheric Maps, GIM, the planetary ionosphere-plasmasphere storms have been identified from the GIM-TEC maps, and they are provided online from 1999 up to present (Gulyaeva and Stanislawska, 2008; 2010). The planetary ionospheric storm Wp index is obtained from the W-index map as a latitudinal average of the distance between maximum positive and minimum negative W-index weighted by the latitude/longitude extent of the extreme values on the map.

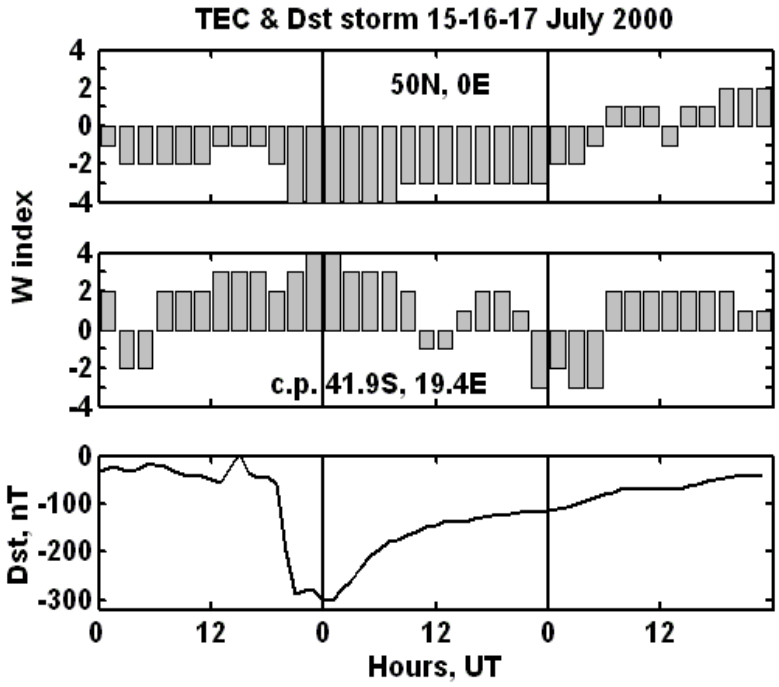

Figure 11. W index of ionospheric weather obtained from TECgps map at two magnetic conjugate locations (upper and middle sections), and magnetic Dst index during the storm on 15-17 July 2000.

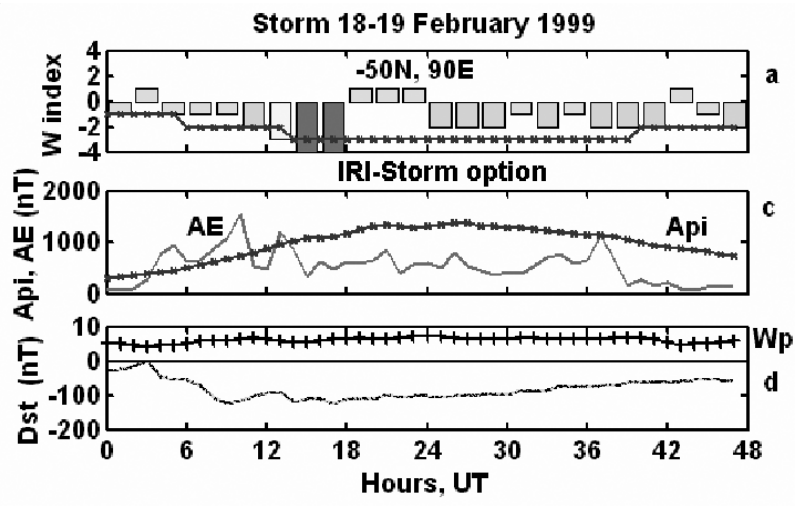

Figure 12. W index of ionospheric weather obtained from TECgps map at [50°S, 90°E] and IRI-Storm prediction (upper section), auroral electrjet AE index and integrated Api magnetic index (middle section), planetary ionospheric Wp index and Dst index (lower section) during the space weather storm on 18-19 February 1999.

The threshold Wp exceeding 4.0 index units and the peak value Wpmax≥6.0 specify the duration and the power of the planetary ionosphere-plasmasphere storm. W index variation during the space weather storm on 18-19 February 1999 is plotted in Figure 12 (upper panel) at [50ºS, 90ºE] accompanied by IRI-Storm prediction (solid curve with asterisks). Geomagnetic Auroral Electrojet AE index and integrated Api index (Fuller-Rowell et al., 2000; Araujo-Pradere et al., 2002) are shown in middle panel. The planetary ionospheric Wp index mirrors variation of Dst index in the lower panel.

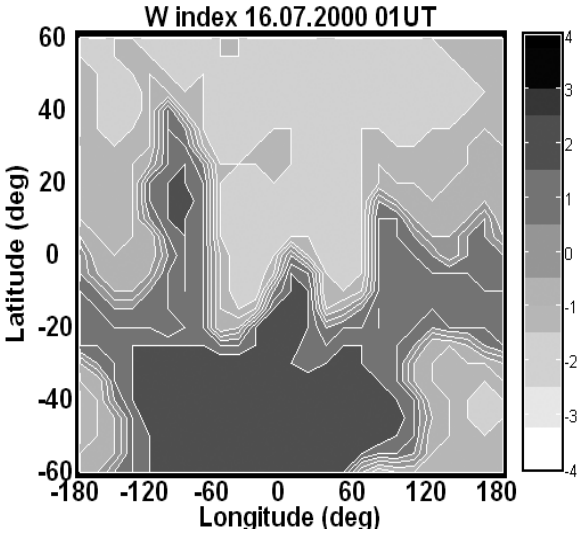

Figure 13. Global map of TEC-based W index during the peak of the space weather storm on 16 July 2000 at 1h UT.

The TEC-based global W index map is calculated at each grid point of TECgps map at latitudes from 60ºS to 60ºN in step of 5º, longitudes from -180º to 180ºE in step of 15º (corresponding to 1h step in local time worldwide). Example of global W index map is given in Figure 13 on 16th July 2000 at the peak of Dst index at 1h UT during the storm (see Figure 11). Prevailing negative storm effects are seen at nighttime in the Northern hemisphere while the positive storm dominated at the Southern hemisphere. Product of W index derived from the F2 layer peak electron density (critical frequency foF2) is provided online in near real time at the Ionospheric Weather page (http://www.izmiran.ru/services/iweather).

It can be calculated and provided along with other IRI standard output parameters (see Table 2) when the IRI-Storm option is used or when IRI is used in data assimilative mode (Fuller-Rowell et al., 2000; 2006; Bilitza, 2001; Gulyaeva et al., 2011).

Conclusion

An international standard for the representation of the Earth's plasma parameters in the ionosphere and plasmasphere is important for a wide spectrum of applications. Examples are Altimetry, Radioastronomy, Satellite Navigation, Communication and Orbit determination. It's usage for HF Communications implies that the electromagnetic waves traveling through the ionosphere and plasmasphere experience a retardation and refractive effect. Implementation of such standard in Space Exploration Industry is needed because a remote sensing technique relying on signals traversing the ionosphere and plasmasphere therefore needs to account for the plasma influence on satellite operation.

The International Reference Ionosphere (IRI), a joint project of URSI and COSPAR, is the de facto international standard for the climatological specification of ionospheric parameters and as such it is currently undergoing registration as Technical Specification (TS16457) of the International Standardization Organization (ISO). Since its first edition in 1969 the IRI model has been steadily improved with newer data and with better mathematical descriptions of global and temporal variation patterns. A large number of independent studies have validated the IRI model in comparisons with direct and indirect ionospheric measurements not used in the model development.

The IRI model is widely used as a tool both in science and eingineering and also for educational purposes for university course materials. Table 4 demonstrates the distriubution of IRI citations in the science literature year-by-year and by institutions in different countries (total number of 699 for the period of 1993 to 2010). A review of acknowledgements of Radio Science papers in 2009 and 2010 showed that during both years 10% of the science papers in this publication acknowledged the use of the IRI model.

While IRI is the internationally accepted standard for the empirical representation of ionospheric parameters, a similar concensus does not yet exist for the plasmasphere. Several modeling approaches have been proposed for extending IRI to plasmaspheric altitudes and the most well established ones are included in this paper. We present comparisons of two of these plasmaspheric models with measurements.

IRI provides one of the better empirical model specifications freely available online for the users. IRI extension above 2000 km is needed, in particular, because the GPS satellites widely used for monitoring the ionosphere nowadays are located at 20,200 km. While the plasma density above 2000 km is at least two (frequently four or more) orders of magnitude

less than the F-region peak density, the altitude range in the plasmasphere above the IRI model is about an order of magnitude greater than the thickness of the ionosphere.

Table 4. Publications in Radio Science related with IRI model

Year	Record count	% of 699		Country / Territory	Record count	% of 699
1993	12	1.7		USA	234	33.5
1994	40	5.7		RUSSIA	77	11.0
1995	45	6.4		INDIA	66	9.4
1996	10	1.4		ITALY	54	7.7
1997	31	4.4		ARGENTINA	51	7.3
1998	28	4.0		JAPAN	51	7.3
1999	33	4.7		PEOPLES R CHINA	46	6.6
2000	10	1.4		ENGLAND	36	5.2
2001	34	4.9		BRAZIL	30	4.3
2002	36	5.2		GERMANY	28	4.0
2003	51	7.3		NIGERIA	28	4.0
2004	52	7.4		CZECH REPUBLIK	26	3.7
2005	27	3.9		POLAND	25	3.6
2006	46	6.6		SOUTH AFRICA	25	3.6
2007	61	8.7		TAIWAN	25	3.6
2008	44	6.3		AUSTRALIA	19	2.7
2009	49	7.0		FRANCE	18	2.6
2010	50	7.2		SPAN	18	2.6
				AUSTRIA	16	2.3
				CANADA	13	1.9
				TURKEY	11	1.6
				BULGARIA	9	1.3

The temporal and spatial variation in ionospheric structures have often frustrated the efforts of communications and radar system operators who base their frequency management decisions on monthly mean predictions of radio propagation in the high frequency (short-wave) band. With the growth of trans-ionospheric and trans-plasmaspheric radio navigation systems, TEC measurements from these systems have become the most numerous ionospheric data set. Treating GPS TEC measurements as the worldwide source of information on the ionosphere and plasmasphere, data assimilative algorithms can more fully determine the spatial structure and dynamics of the space plasma environment. The particular model parameters such as F2 layer peak electron density and total electron content adjusted to observation allows to express the ionospheric weather from quiet state to severe storm by ionospheric W-index characterizing ionosphere and plasmasphere state retrieved from deviation of instant value from the reference median value.

The ionospheric plasma density distribution and TEC depend on a number of upper atmospheric and ionospheric parameters, such as the neutral density, neutral wind, neutral and plasma temperatures, plasmaspheric flux, and ion-neutral collision frequencies. Considerable efforts are currently expended on the development and promotion of assimilative algorithms that allow to combine a physical or empirical model with measured data, and thus allow

adapting the model to real-time conditions. In the numerical physical modeling of the ionosphere these assimilative inputs are often only roughly known and can cause significant uncertainties in the physical model results (Jee et al., 2005). The promotion of the empirical IRI model to a full international standard is well justified by the reliability and accuracy of IRI output parameters and the public availability of IRI code for the worldwide user community. Added benefits are the user-friendly interface for online calculation of IRI standard parameters, and the availability of guidance materials for newcomers helping with implementation and adapting of IRI system to the particular user's needs. The high degree of acceptance of IRI in the heliospheric and geospheric community is also the fact that IRI is used as the reference model for determining the skill score of evolving physical models, e.g., for the CEDAR challenge and for the CCMC (Sojka et al., 2007).

It is expected that the significant contributions to international collaboration and coordinated input relative to space vehicle design and operations, plasma environment specification, and communication and navigation services will result from the promotion of this proposed ISO Standard.

APPENDIX: Model Availability

The IRI homepage is at http://IRI.gsfc.nasa.gov. From this page the user has access to information about the model, to the Fortran code (http://nssdcftp.gsfc.nasa.gov/models /ionospheric/iri/) and to a web interface for computation, listing, and plotting of model parameters (http://omniweb.gsfc.nasa.gov/vitmo/iri_vitmo. html). The Fortran code and IRI interface are also accessible from the Community Coordinated Modeling Center (CCMC; http://ccmc.gsfc.nasa.gov/requests/requests.php).

A FORTRAN code implementation of GCPM that includes all except the polar cap is available from dennis.gallagher@msfc.nasa.gov.

The GPID model source code was written using commercial MATLAB software, but is not currently available for release.

Source code for the IZMIRAN IRI ionosphere-plasmasphere version is available from the IZMIRAN web site ftp://ftp.izmiran.ru/pub/izmiran/SPIM/.

Acknowledgments

The IRI model is the result of modeling efforts by a group of ionospheric experts that form the IRI Working Group of the Committee of Space Research (COSPAR) and the International Union of Radio Science (URSI). The efforts by this group are greatly appreciated and we are thankful to COSPAR and URSI for sponsoring this activity. TLG acknowleges the support of the joint grant from RFBR (Project 11-02-91370-CT_a) and TUBITAK (Project EEEAG 110E296) for this work and DB acknowledges support through NASA grants NNX09AJ74G and NNX07A065G and NSF grant AGS-0819440. The ISO/TS16457:2009 Document is provided at (http://www.iso.org /iso/iso_catalogue/catalogue_tc/catalogue_detail.htm? csnumber=51248:). Global Ionospheric Maps, TECgps, and TOPEX data are provided online at (ftp://cddis.gsfc.nasa.gov/pub/gps/products/ionex/).

References

Altadill, D., Arrazola, D., Blanch, E., Buresova, D. Solar activity variations of ionosonde measurements and modeling results, *Adv. Space Res.* 42, 610–616, 2008.

Altadill, D., Torta, J.M., Blanch, E. Proposal of new models of the bottom-side B0 and B1 parameters for IRI, *Adv. Space Res.* 43, 1825 -1834, doi:10.1016/j.asr.2008.08.0144, 2009.

Angling, M.J., Cannon, P.S. Assimilation of radio occultation measurements into background ionospheric models. *Radio Sci*. 39, doi:10.1029/2002RS002819, 2004.

Araujo-Pradere, E.A., Fuller-Rowell, T.J., Codrescu, M.V. STORM: An empirical storm-time ionospheric correction model. 1. Model description. *Radio Sci*., 37(5), 1070, doi:10.1029/2001RS002467, 2002.

Arikan, O., Arikan, F., Erol, C.B. Computerized ionospheric tomography with the IRI model. *Adv. Space Res.*, 39, 859–866, doi:10.1016/j.asr.2007.02.078, 2007.

Bailey, G.J., Balan, N. and Su, Y.Z. The Sheffield University plasmasphere ionosphere model—A review, *J. Atmos. Sol. Terr. Phys*., 59, 1541–1552, 1997.

Bent, R.B., Llewellyn, S.K., Walloch, M.K. *SAMSO TR-72-239*, Space and Missile Systems Organization, Los Angeles, California 90045, 1972.

Bilitza, D., Electron density in the D-region as given by the International Reference Ionosphere, World Data Center A for Solar-Terrestrial Physics, *Report UAG-82*, 7-11, 1981.

Bilitza, D., Sheikh, N.M., Eyfrig, R. A global model for the height of the F2 peak using M3000 values from the CCIR. *Telecomm. J.*, 46, 549-553, 1979.

Bilitza, D., Rawer, K. New options for IRI electron density in the middle ionosphere. *Ady. Space Res.* 10(11), (11)7-(11)16, 1990.

Bilitza, D., Rawer, K., Bossy, L., Gulyaeva, T.. International Reference Ionosphere - Past, Present, and Future: I. Electron density. *Ady. Space Res.* 13(3), (3)3-(3)13, 1993a.

Bilitza, D., Rawer, K., Bossy, L., Gulyaeva, T.. International Reference Ionosphere - Past, Present, and Future: II. Plasma temperatures, ion composition and ion drift. *Adv. Space Res.* 13, N 3, 15–23, 1993b.

Bilitza, D., S. Radicella, B. Reinandh, J. Adeniyi, M. Mosert de Gonzalez, S. Zhang, and 0. Obrou, New B_0 and B_1 models for IRI, *Adv. Space Res.,* 25(l)*,* 89-96, 2000.

Bilitza D. International Reference Ionosphere 2000, *Radio Science.* 36, 261–275, 2001.

Bilitza, D., Reinisch, B., Benson, R., Grebowsky, J., Papitashvili, N., Huang, X., Schar, W., Hills, K. Online data base of satellite sounder and in situ measurements covering two solar cycles. *Adv. Space Res.* 31(3), 769-774, 2003.

Bilitza, D. A correction for the IRI topside electron density model based on Alouette/ISIS topside sounder data. *Adv. Space. Res.* 33(6), 838–843, 2004.

Bilitza, D., Reinisch, B.W., Radicella, S.M., Pulinets, S., Gulyaeva, T., Triskova, L. Improvements of the IRI model for the topside electron density profile. *Radio Sci.,* 41(5), RS5S15, doi:10.1029/2005RS003370, 2006.

Bilitza, D., Truhlik, V., Richards, P., Abe, T., Triskova, L. Solar cycle variation of mid-latitude electron density and temperature: Satellite measurements and model calculations, *Adv. Space Res*., 39(5), 779-789, doi: 10.1016/j.asr.2006.11.022, 2007.

Bilitza, D., Reinisch, B.W. International Reference Ionosphere 2007: Improvements and new parameters. *Adv. Space Res.* 42, 599-609, doi:10.1016/j.asr.2007.07.048, 2008.

Bilitza, D. Evaluation of IRI-2007 model options for the topside electron density. *Adv. Space Res*., 44 (8), 701-706, doi:10.1016/j.asr.2009.04.036, 2009.

Bremer, J., Cander, Lj. R., Mielich, J., Stamper, R. Derivation and test of ionospheric activity indices from real-time ionosonde observations in the European region. *J. Atmos. Sol.-Terr. Phys.*, 68, 2075–2090, 2006.

Bust, G.S., Coker, C., Coco, D.S., Gaussiran II, T.L., Lauderdale, T. IRI data ingestion and ionospheric tomography. *Adv. Space Res.* 27, 157–165, 2001.

Bust, G.S, Garner, T.W., Gaussiran II, T.L. Ionospheric Data Assimilation Three Dimensional (IDA3D): A Global, Multi-Sensor, Electron Density Specification Algorithm, *J. Geophys. Research*, 109, A11312, doi:10.1029/2003JA010234, 2004.

Bust, G.S., Mitchell, C.N. History, current state, and future directions of ionospheric imaging. *Rev. Geophys*. 46, RG1003, doi:10.1029/2006RG000212, 2008.

Carpenter, D.L., Park, C.G. On what ionospheric workers should know about the plasmapause – plasmasphere. *Rev. Geophys. Space Phys*., 11, 133-154, 1973.

CCIR, *Atlas of ionospheric characteristics*, Comite Consultatif International des Radio Communications, Rep. 340, International Telecommunication Union, Geneve, 1983.

Chasovitin, Yu.K., Gulyaeva, T.L., Deminov, M.G., Ivanova, S.E. Russian standard model of ionosphere (SMI). In *COST251TD(98)005*, RAL, UK, 161-172, 1998.

Chu, Y.-H., Wu, K.-H., Su, Ch.-L. A new aspect of ionospheric E region electron density morphology. *J. Geophys. Res.*, 114, A12, A12314, DOI:10.10292008JA014022, 2009.

Coisson, P., Radicella, S.M., Nava, B. Comparisons of experimental topside electron concentration profiles with IRI and NeQuick models. *Ann. Geophys.* 45 (1), 125–130, 2002.

Coisson, P., Radicella, S.M., Leitinger, R., Nava, B. Topside electron density in IRI and NeQuick: features and limitations. *Adv. Space Res.* 37 (5), 934–937, 2006.

Cueto, M., Coisson, P., Radicella, S.M., Herraiz, M., Ciraolo, L., Brunini, C. Topside ionosphere and plasmasphere: Use of NeQuick in connection with Gallagher plasmasphere model. *Adv. Space. Res.*, 39, 739–743, doi:10.1016/j.asr.2007.01.073, 2007.

Danilov, A.D., Semenov, V.K. Relative ion composition model at midlatitudes, *J. Atmos. Terr. Phys.*, 40, 1093, 1978.

Danilov, A.D., Yaichnikov, A.P. A New Model of the Ion Composition at 75 to 1000 km for IRI, *Adv. Space Res.* 5(7), 75-79, 107-108, 1985.

Danilov, A.D., Smirnova, N.V. Improving the 75 to 300 km ion composition model of the IRI, *Adv. Space Res.* 15(2), 171-177, 1995.

Danilov, A., Rodevich, A. Smirnova, N. Problems with incorporating a new D-region model into the IRI, *Adv. Space Rex,* 15(2), 165-169, 1995.

Ducharme, E.D., Petrie, L.E., Eyfrig, R. A method for predicting the F1-layer critical frequency. *Radio Sci.*, 6, 369-378, 1971; *Radio Sci.*, 8, 837-839, 1973.

Dudeney, J.R. A Simple Empirical Method for Estimating the Height of the F2-Layer at the Argentine Islands Graham Land, *Science Report No.* 88, London, UK, British Antarctic Survey, 1974.

Fejer, B.G. Low latitude electrodynamic plasma drifts: A review, *J. Atmos. Terr. Phys.*, 53, 677–693, 1991.

Fernandez J.R., Mertens, C.J., Bilitza, D., Xu, X., Russell III, J.M., Mlynczak, M.G. Feasibility of developing an ionospheric E-region electron density storm model using TIMED/SABER measurements, *Adv. Space Res.* 46(8), 1070-1077, doi:10.1016/j.asr.2010.06.008, 2010.

Field, P.R., Rishbeth, H. The response of ionospheric F2-layer to geomagnetic activity: an analysis of worldwide data, *J. Atmos. Sol.-Terr. Phys.*, 59, 2, 163–180, 1997.

Foster, J.C., Holt, J.M., Musgrove, R.G., Evans, D.S. Ionospheric convection associated with discrete levels of particle precipitation. *Geophys. Res. Letters* 13, 656–659, doi:10.1029/GL013i007p00656, 1986.

Friedrich, M., Torkar, K. FIRI: A semiempirical model of the lower ionosphere, *J. Geophys. Res.,* 106, Al0, 21409-21418, 200l.

Friedrich, M., Pilgram, R., Torkar, K. A novel concept for empirical D-region modelling. *Adv. Space Res.*, 27(1), 5-12, 2001.

Fu, L.L., Christensen, E.J., Yamarone Jr, C.A. TOPEX/Poseidon mission overview, *J. Geophys. Res.*, 99, 24369–24381, 1994.

Fuller-Rowell, T.J., Evans, D.S. Height-integrated Pedersen and Hall conductivity patterns inferred from the TIROS-NOAA satellite data, *J. Geophys. Res.*, 92, 7606–7618, 1987.

Fuller-Rowell, T.J., D. Rees, S. Quegan, R.J. Moffett, M.V. Codrescu, G.H. Millward, *STEP Handbook of Ionospheric Models*, edited by R.W. Schunk, Utah State Univ.,1996.

Fuller-Rowell T.J., Araujo-Pradere E.A., Codrescu M.V. An Empirical Ionospheric Storm-Time Correction Model. *Adv. Space Res.*, 25(1), 139-146, doi: 10.1016/S0273-1177(99)00911-4, 2000.

Fuller-Rowell, T.J., Codrescu, M.V., Araujo-Pradere, E.A. Capturing the storm-time ionospheric response in an empirical model. *AGU Geophys. Monograph,* 125, 393-401, 2001.

Fuller-Rowell, T., Araujo-Pradere, E.A., Minter, C., Codrescu, M. , Spencer, P., Robertson, D., Jacobson, A. R. US-TEC: A new data assimilation product from the Space Environment Center characterizing the ionospheric total electron content using real-time GPS data, *Radio Sci.*, 41, RS6003, doi:10.1029/2005RS003393, 2006.

Gallagher, D.L., Craven, P.D., Comfort, R.H.. Global Core Plasma Model. *J. Geophys. Res*., 105, A8, 18819-18833, 2000.

Gulyaeva T.L. Progress in ionospheric informatics based on electron density profile analysis of ionograms. *Adv. Space Res.* 7, No.6, 39-48, 1987.

Gulyaeva ,T. L.: Logarithmic scale of the ionosphere disturbances, *Geomagn. Aeronomy*, 36, 1, 115–118, 1996.

Gulyaeva T.L., Huang, X., Reinisch, B.W. Plasmaspheric extension of topside electron density profiles. *Adv. Space Res.,* 29, No.6, 825-831, 2002a.

Gulyaeva T.L., Huang, X., Reinisch, B.W. Ionosphere-Plasmasphere Model Software for ISO. *Acta Geod. Geophys. Hungarica,* 37, Nos. 2-3, 143-152, 2002b.

Gulyaeva, T. L.: Daily assessment of the ionosphere variability, *Acta Geod. Geophys. Hungarica*, 37(2–3), 303–308, 2002c.

Gulyaeva, T.L. Variations in the half-width of the topside ionosphere according to the observations of space ionosondes ISIS 1, ISIS 2, and IK19, *Int. J. Geomagn. Aeron.* 4(3), 201-207, 2003.

Gulyaeva, T.L., Titheridge, J.E. Advanced specification of electron density and temperature in the IRI ionosphere-plasmasphere model. *Adv. Space Res.*, 38(11), 2587-2595, doi:10.1016/j.asr.2005.08.045, 2006.

Gulyaeva T.L. Variable coupling between the bottomside and topside thickness of the ionosphere. *J. Atmos. Solar-Terr. Phys.,* 69(4-5), 528-536, doi:10.1016/j.jastp.2006.10.015, 2007.

Gulyaeva, T.L., Gallagher, D.L. Comparison of two IRI electron-density plasmasphere extensions with GPS-TEC observations. *Adv. Space Res.*, 39, 744-749, doi:10.1016/j.asr.2007.01.064, 2007.

Gulyaeva, T.L., Stanislawska, I. Derivation of a planetary ionospheric storm index. *Annales Geophysicae*, 26, N.9, 2645-2648, 2008.

Gulyaeva, T.L., Arikan, F., Delay, S. Scale factor mitigating non-compliance of double frequency altimeter measurements of the ionospheric electron content over the oceans with GPS-TEC maps. *Earth, Planets and Space*, 61, 1103-1109, 2009.

Gulyaeva, T.L., Stanislawska, I. Magnetosphere associated storms and autonomous storms in the ionosphere-plasmasphere environment. *J. Atmos. Solar-Terr. Phys.*, 72, 90-96, doi:10.1016/j.jastp.2009.10.012 , 2010.

Gulyaeva, T.L., Arikan, F., Stanislawska, I. Inter-hemispheric Imaging of the Ionosphere with the upgraded IRI-Plas model during the space weather storms. *Earth, Planets and Space*, 2011.

Gulyaeva T.L. Storm time behavior of topside scale height inferred from the ionosphere-plasmasphere model driven by the F2 layer peak and GPS-TEC observations. *Adv. Space Res.*, 47, 913-920, doi:10.1016/j.asr.2010.10.025, 2011a.

Gulyaeva, T.L. Storm-time model of the ionosphere peak height associated with changes of peak electron density. *Adv. Space Res.*, 2011b (submitted).

Hajj, G. A., Wilson, B.D., Wang, C., Pi, X., and Rosen, I.G. Data assimilation of ground GPS total electron content into a physics-based ionospheric model by use of the Kalman filter, *Radio Sci.*, 39, RS1S05, doi:10.1029/2002RS002859, 2004,.

Hedin, A.E. Extension of the MSIS thermosphere model into the middle and lower atmosphere, *J. Geophys. Res.*, 96, 1159–1172, 1991.

Hedin, A.E., Fleming, E.L., Manson, A.H., Schmidlin, F.J., Avery, S.K., et al. Empirical wind model for the upper, middle and lower atmosphere, *J. Atmos. Terr. Phys.*, 58, 1421–1447, 1996.

Heelis, R.A., Lowell, J.K., and Spiro, R.W. A Model of the High-Latitude Ionospheric Convection Pattern. *J. Geophys. Res*. 87, A8, 6339-6345, doi:10.1029/JA087iA08p06339, 1982.

Heise, S., Jakowski, N., Wehrenpfennig, A., Reigber, Ch., Luehr, H. Sounding of the topside ionosphere/plasmasphere based on GPS measurements from CHAMP: initial results. *Geophys. Res. Lett.* 29 (14), doi:10.1029/2002GL014738, 2002.

Heppner, J.P., Maynard, N.C. Empirical high-latitude electric field models, *J. Geophys. Res.*, 92, 4467-4489, 1987.

Hochegger, G., Nava, B., Radicella, S.M., Leitinger, R. A family of ionospheric models for different uses. *Phys. Chem. Earth (C)*, 25 (4), 307–310, doi:10.1016/S1464-1917(00)00022-2, 2000.

Huang, X., Reinisch, B.W., Song, P., Nsumei, P., Green, J.L., Gallagher, D.L. Developing an empirical density model of the plasmasphere using IMAGE/RPI observations, *Adv. Space Res.*, 33, 6, 829-832, 2004.

Hysell, D.L. Inverting ionospheric radio occultation measurements using maximum entropy, *Radio Sci.*, 42, RS4022, doi:10.1029/2007RS003635, 2007.

Iwamoto, L., Katoh, H., Maruyama, T., Minakoshi, H., Watari, S., Igarashi, I. Latitudinal variation of solar flux dependence in the topside plasma density: comparison between IRI model and observations. *Adv. Space Res*. 29 (6), 877–882, 2002.

Jakowski, N., Stankov, S.M., Schlueter, S., Klaehn, D. On developing a new ionospheric perturbation index for space weather operations. *Adv. Space Res.*, 38(11), 2596-2600, doi:10.1016/j.asr.2005.07.043, 2006.

Jee, G., Schunk, R.W., Scherliess, L. On the sensitivity of total electron content (TEC) to upper atmospheric / ionospheric parameters. *J. Atmos. Terr. Phys.*, 67(11), 1040-1052, 2005.

Jorgensen, A.M., Ober, D., Koller, J., Friedel, R.H.W. Specification of the Earth's plasmasphere with data assimilation. *Adv. Space Res.*, doi:10.1016/ j.asr.2010.06.013, 2010.

Kelley, M.C., Wong, V.K., Aponte, N., Coker, C., Mannucci, A.J., and Komjathy, A. Comparison of COSMIC occultation-based electron density profiles and TIP observations with Arecibo incoherent scatter radar data, *Radio Sci*., 44, RS4011, doi:10.1029/2008RS004087, 2009.

Kotova, G.A. The Earth's Plasmosphere: current state of research. *Geomagnetism and Aeronomy*, 47(4), 1-16, 2007.

Kouris, S.S., Muggleton, L.M. Diurnal variation in the E-layer ionization. *J. Atmos. Terr. Phys.*, 35, 133-137, 1973.

Kouris, S. S., Fotiadis, D. N., Zolesi, B. Specifications of the F region variations for quiet and disturbed conditions, *Phys. Chem. Earth, Part C*, 24(4), 321–327, 1999.

Kutiev, I. and Muchtarov, P. Modeling of midlatitude F-region response to geomagnetic activity, *J. Geophys. Res*., 106, 15 501–15 509, 2001.

Liu, J.Y., Lin, C.Y., Lin, C.H., Tsai, H.F., Solomon, S.C., Sun, Y.Y., Lee, I.T., Schreiner, W.S., Kuo, Y.H. Artificial plasma cave in the low-latitude ionosphere results from the radio occultation inversion of the FORMOSAT-3/COSMIC, *J. Geophys. Res.*, 115, A07319, doi:10.1029/2009JA015079, 2010.

Llewellyn, S.K., Bent, R.B. Documentation and description of the Bent ionospheric model, *Rep. AFCRL-TR-73-0657*, Air Force Cambridge Res. Lab., Hanscom AFB, Bedford, Mass., 1973.

McKinnell, L.A., Friedrich,M., Steiner, R.J. A new approach to modeling the daytime lower ionosphere at auroral latitudes. *Adv. Space Res.* 34(9), 1943–1948, 2004.

McKinnel, L.A., Friedrich, M. Results from a new lower ionosphere model. *Adv. Space Res.* 37 (5), 1045–1050, 2006.

McKinnell, L.A., Oyeyemi, E.O. Progress towards a new global foF2 model for the International Reference Ionosphere (IRI). *Adv. Space Res.*, 43(11), 1770-1775, doi:10.1016/j.asr.2008.09.035, 2009.

McKinnell, L.A., Oyeyemi, E.O. Equatorial predictions from a new neural network based global foF2 model. *Adv. Space Res.*, 46 (8), 1016-1023, doi:10.1016/j.asr.2010.06.003, 2010.

Mechtley, E., Bilitza, D. Models of D-region electron concentration, *Rep. IPW-WB 1*, Institut fur physikalische Weltraumforschung, Freiburg, Germany, 1974.

Menveielle, M., Berthelier, A. The K-derived planetary indices: description and availability, *Rev. Geophys*., 29(3), 415–432, 1991.

Millward, G.H., Moffett, R.J., Quegan, S., Fuller-Rowell, T.J. "A Coupled Thermosphere Ionosphere-Plasmasphere Model, CTIP," *STEP Handbook of Ionospheric Models*, edited by R.W. Schunk, Utah State Univ, 1996.

Nicolls, M.J., Vlasov, M.N., Kelley, M.C., Shepherd, G.D. Discrepancy between the nighttime molecular ion composition given by the international reference ionosphere model and airglow measurements at low latitudes, *J. Geophys. Res.*, 111, A03304, doi:10.1029/ 2005JA011216, 2006.

Nsumei, P.A., Huang, X., Reinisch, B.W., Song, P., Vasyliunas, V.M., Green, J.L., Fung, S.F., Benson, R.F., and Gallagher, D.L. Electron Density Distribution Over the Northern Polar Region Deduced from IMAGE/RPI Sounding, *J. Geophys. Res.*, 108, A2, 2003

Oyeyemi, E.O., McKinnell, L.A., Poole, A.W.V. Neural network-based prediction techniques for global modeling of M(3000)F2 ionospheric parameter. Adv. Space Res., 39(5), 643-650, doi:10.1016/j.asr.2006.09.038, 2007.

Oyeyemi, E.O., McKinnell, L.A. A new global F2 peak electron density model for the International Reference Ionosphere (IRI). *Adv. Space Res*., 42(4), 645-658, doi:10.1016/j.asr.2007.10.031, 2008.

Pi, X., Wang, C., Hajj, G.A. , Rosen, G. , Wilson, B.D., Bailey, G. J. Estimation of ExB drift using a global assimilative ionospheric model: An observation system simulation experiment, *J. Geophys. Res.*, 108(A2), 1075, doi:10.1029/2001JA009235, 2003.

Picone, J.M., Hedin, A.E., Drob, D.P., Aikin, A.C. NRLMSIS00 empirical model of the atmosphere: Statistical comparisons and scientific issues, *J. Geophys. Res.*, 107(A12), 1468, doi:10.1029/2002JA009430, 2002.

Radicella, S.M., Leitinger, R. The evolution of the DGR approach to model electron density profiles. *Adv. Space Res.* 27 (1), 35–40, 2001.

Raeder J., Larson D., Li W., Kepko E.L., and Fuller-Rowell T. Open GGCM Simulations for the THEMIS Mission. *Space Science Review*, 141(1-4), 535-555, 2008.

Ramakrishnan, S., Rawer, K. Model electron density profiles obtained by empirical procedures, *Space Research* XII, 1253-1259, Akademie Verlag, Berlin, German Democratic Republic, 1972.

Rawer, K. *Meteorological and Astronomical Influences on Radio Wave Propagation*, ed. B. Landmark, Pergamon Press., Oxford, pp.221-250, 1963.

Rawer, K., Ramakrishnan, S., Bilitza, D.. Preliminary Reference profiles of Electron and Ion Densities and Temperatures, Institute for Space Research, *Report IPW-WB2,* Freiburg, Germany, 1972.

Rawer, K., Ramakrishnan, S., Bilitza, D. International Reference Ionosphere 1978, International Union of Radio Science, *Special Report*, Brussels, Belgium, 1978.

Rawer, K. New description of the electron density profile. *Adv. Space Res.*, 4(1), 11-15, 1984.

Rawer, K. Data needed for an analytical description of the electron density profile. *Adv. Space Res.*, 11(10), (10)57-(10)65, 1991.

Reinisch, B., Huang, X. Redefining the IRI F1 Layer profile, *Adv. Space Res,* 25(l), 81-88, 1999.

Reinisch, B.W., Haines, D.M., Bibl, K., Cheney, G., Galkin, I.A., Huang, X., Myers, S.H., Sales, G.S., Benson, R.F., Fung, S.F., Green, J.L., Boardsen, S., Taylor, W.W.L., Bougeret, J.-L., Manning, R., Meyer-Vernet, N., Moncuquet, M., Carpenter, D.L., Gallagher, D.L., and Reiff, P. The Radio Plasma Imager investigation on the IMAGE spacecraft, *Space Science Reviews*, 91, pp. 319-359, 2000.

Reinisch, B.W., Huang, X., Song, P., Green, J.L., Fung, S.F., Vasyliunas, V.M., Gallagher, D.L., Sandel, B.R. Plasmaspheric mass loss and refilling as a result of a magnetic storm, *J. Geophys. Res*., 109, A1, A01202, 1-11, doi:10.1029/2003JA009948, 2004

Reinisch, B.W., Nsumei, P., Huang, X., Bilitza, D.K. Modeling the F2 topside and plasmasphere for IRI using IMAGE/RPI and ISIS data. *Adv. Space Res.* 39 (5), 731–738, 2007.

Richards, P.G. The Field Line Interhemispheric Plasma Model. In: *Solar-Terrestrial Energy Program: Handbook of Ionospheric Models*, edited by R.W. Schunk, p. 207, 1996.

Richards, P.G. Ion and neutral density variations during ionospheric storms in September 1974: comparison of measurement and models. *J. Geophys. Res.* 107 (A11), 1361, doi:10.1029/2002JA009278, 2002.

Richards, P.G., Bilitza, D., and Voglozin, D. Ion density calculator (IDC): A new efficient model of ionospheric ion densities, *Radio Sci.*, 45, RS5007, doi:10.1029/2009RS004332, 2010.

Richmond, A.D., Blanc, M., Emery, B.A., Wand, LH., Fejer, B.G., Woodman, R.F., Ganguly, S., Amayenc, P., Behnke, R.A., Calderon, C., and Evans, J.V. An Empirical Model of Quiet-Day Ionospheric Electric Fields at Middle and Low Latitudes. *J. Geophys. Res.* 85, A9, 4658-4664, doi:10.1029/JA085iA09p04658, 1980.

Rishbeth, H., Garriott, O.K. Introduction to ionospheric physics, Academic Press, New York, 331pp., 1969.

Roble, R.G., Ridley, E.C., Richmond, A.D. A Coupled Thermosphere/Ionosphere general circulation model. *Geophys. Res. Lett.*, 15(12), 1325-1328, 1988.

Rodger, A.S., Wrenn, G.L., Rishbeth, H. Geomagnetic storms in the Antarctic F region, II, physical interpretation, *J. Atmos. Terr. Phys*., 51, 851-866 1989.

Rush, C., Fox, M., Bilitza, D., Davies, K., McNamara, L., Stewart, F., PoKempner, M. Ionospheric mapping – An update of foF2 coefficients. *Telecomm. J*., 56, 179-182, 1989.

Scherliess, L., Fejer, B.G. Radar and satellite global equatorial F region vertical drift model, *J. Geophys. Res.*, 104, 6829–6842, 1999.

Scherliess, L., Schunk, R.W., Sojka, J.J., Thompson, D.C. Development of a physics-based reduced state Kalman filter for the ionosphere, *Radio Sci.*, 39, RS1S04, doi:10.1029/2002RS002797, 2004.

Schunk, R.W., Nagy, A.F. *Ionosphere: Physics, Plasma Physics, and Chemistry*, Cambridge, New York, pp. 333-335, 2000.

Sojka, J.J., Thompson, D.C., Scherliess, L., Schunk, R.W., Harris, T.J. Assessing models for ionospheric weather specifications over Australia during the 2004 Climate and Weather of the Sun-Earth-System (CAWSES) campaign, *J. Geophys. Res.*, 112, A09306, doi:10.1029/2006JA012048, 2007.

Stankov, S.M., Jakowski, N., Heise, S., Muhtarov, P., Kutiev, I., Warnant, R. A new method for reconstruction of the vertical electron density distribution in the upper ionosphere and plasmasphere. *J. Geophys. Res.* 108, doi:10.1029/2002JA009570, 2003.

Tobiska, W.K. Revised solar extreme ultraviolet flux model, *J. Atmos. Terr. Phys.*, 53, 1005–1018, 1991.

Triskova, L., Truhlik, V., Smilauer, J. An empirical model of ion composition in the outer ionosphere. *Adv. Space Res.* 31 (3), 653–663, 2003.

Truhlik, V., Triskova, L., Smilauer, J., Afonin, V. Global empirical model of electron temperatures in the outer ionosphere for period of high solar activity based on data of three Intercosmaos satellites, *Adv. Space Res*., 25(1), 163-172, 2000.

Truhlik, V., Triskova, L., Smilauer, J. New advances in empirical modeling of ion composition in the outer ionosphere. *Adv. Space Res.* 33, 844–849, 2004.

Truhlik V., Triskova, L., Bilitza, D., Podolska, K. Variations of daytime and nighttime electron temperature and heat flux in the upper ionosphere, topside ionosphere and lower plasmasphere for low and high solar activity, *J. Atmos. Sol.-Terr. Phys.* 71, 2055–2063, doi:10.1016/j.jastp.2009.09.013, 2009.

Vergados, P., Pagiatakis, S.D. First estimates of the second-order ionospheric effect on radio occultationobservations, *J. Geophys. Res.*, 115, A07317, doi:10.1029/2009JA015161, 2010.

Vlasov, M.N., Kelley, M.C. Crucial discrepancy in the balance between extreme ultraviolet solar radiation and ion densities given by the international reference ionosphere model, *J. Geophys. Res.*, 115, A08317, doi:10.1029/2009JA015103, 2010.

Wang, C., Hajj, G., Pi, X., Rosen, I.G., Wilson, B. Development of the Global Assimilative Ionospheric Model. *Radio Sci.* 39, doi:10.1029/2002RS002854, 2004a.

Wang, W., Wiltberger, M., Burns, A.G., Solomon, S.C., Killeen, T.L., Maruyama, N., Lyon, J.G. Initial results from the coupled magnetosphere-ionosphere-thermosphere model: thermosphere-ionosphere responses. *J. Atmos. Solar-Terr. Phys.*, 66(15-16), 1425-1441, doi:10.1016/j.jastp.2004.04.008, 2004b.

Webb, P.A., Essex, E.A. An ionosphere-plasmasphere global electron density model. *Phys. Chem. Earth (C)*, 25, No. 4, pp. 301-306, 2000.

Webb, P.A., Essex, E.A. A dynamic global model of the plasmasphere. *J. Atmos. Solar-Terr. Phys.*, 66(12), 1057-1073, doi:10.1016/j.jastp.2004.04.001, 2004.

Yizengaw, E., Moldwin, M.B., Galvan, D., Iijima, B.A., Komjathy, A., Mannucci, A.J. Global plasmaspheric TEC and its relative contribution to GPS TEC. *J. Atmos. Sol. Terr. Phys.* 70, 1541–1548, 2008.

Zhang, S.-R., Holt, J.M., van Eyken, A.P., McCready, M., Amory-Mazaudier, C., Fukao, S., Sulzer, M. Ionospheric local model and climatology from long-term databases of multiple incoherent scatter radars. *Geophys. Res. Lett.* 32, L20102, doi:10.1029/2005GL023603, 2005.

Zhang Y-L., Paxton, L.J., Bilitza, D. Near real-time assimilation of auroral peak E-region density and equatorward boundary in IRI. *Adv. Space Res.* 46(8), 1055-1063, doi:10.1016/j.asr.2010.06.029, 2010.

Referred by Lee-Anne McKinnell, lmckinnell@sansa.org.za (a) South African National Space Adency, Hermanus, South Africa (b) Department of Physics and Electronics, Rhodes University, Grahamstown, South Africa.